Calibration Signal-Assisted Emitter Localization Under Sensor Position Uncertainty

MING-YI YOU
No.36 Research Institute of CETC, Jiaxing, China

WENQIANG PU, Member, IEEE
RUI ZHOU, Member, IEEE
Shenzhen Research Institute of Big Data, Shenzhen, China

YUN-XIA YE
No.36 Research Institute of CETC, Jiaxing, China

MINRUI XIAO
Shanghai Jiaotong University, Shanghai, China

WEI WANG
No.36 Research Institute of CETC, Jiaxing, China

QINGJIANG SHI, Member, IEEE
Tongji University, Shanghai, China

The uncertainty of sensor position significantly compromises the accuracy of source localization within the direct position determination (DPD) framework. This article explores the use of an external calibrator that emits a calibration signal with a known position to mitigate the impact of sensor position uncertainty on localization accuracy. By utilizing the calibration signal, we develop a refined Gibbs sampling algorithm as the initial step to effectively address the high-dimensional optimization problem associated with sensor position calibration. In the second step, we account for measurement noise and estimation uncertainties in the calibrated sensor positions and propose a revised DPD method, which demonstrates greater resilience to sensor position uncertainty compared to existing methods. We also derive the Cramer–Rao lower bound for emitter position under scenarios both with and without an external calibrator. Numerical simulations are performed to evaluate the performance of our proposed algorithms against several benchmark methods, demonstrating the effectiveness of our approach.

Received 13 June 2024; revised 17 October 2024 and 6 January 2025; accepted 13 January 2025. Date of publication 24 January 2025; date of current version 11 June 2025.

DOI. No. 10.1109/TAES.2025.3532247

Refereeing of this contribution was handled by G. Wang.

This work was supported in part by the National Natural Science Foundation of China under Grant 62101350 and Grant 62201362, in part by Shenzhen Science and Technology Program under Grant RCBS20221008093126071, and in part by Starlit South Lake Leading Elite Program.

Authors' addresses: Ming-Yi You, Yun-Xia Ye, and Wei Wang are with the National Key Laboratory of Electromagnetic Space Security, No.36 Research Institute of CETC, Jiaxing 314033, China; Wenqiang Pu and Rui Zhou are with the Shenzhen Research Institute of Big Data, The Chinese University of Hong Kong-Shenzhen, Shenzhen 518172, China; E-mail: (wenqiangpu@cuhk.edu.cn); Minrui Xiao is with the School of Sensing Science and Engineering, Shanghai Jiaotong University, Shanghai 200240, China; Qingjiang Shi is with the School of Software Engineering, Tongji University, Shanghai 200070, China. *(Corresponding author: Wenqiang Pu.)*

I. INTRODUCTION

Determining a source location from its emitted signals collected by a sensor network has been of tremendous interest for both academic researchers and industrial practitioners [1], [2], [3], [4], [5]. Typical source localization algorithms are done in two steps. In the first step, location-related parameters are extracted from the received signals, which are critical markers related to the source's location. Typical location-related parameters include Doppler shifts [6], angle of arrival (AoA) [7], time of arrival [8], [9], time difference of arrival (TDOA) [10], frequency difference of arrival [11], [12], [13], received signal strength [14], [15], or a combination of them. The second step involves estimating the source location by utilizing an estimator that seeks to match the extracted parameters. This typically involves solving an optimization problem where the objective function is formulated based on the statistical assumption of the location-related parameters; typical optimization criteria include least squares, maximum likelihood, and Bayesian estimation.

Despite these different criteria, one predominant challenge comes from measurement noise, especially when the SNR is low [16], [17]. In this case, classical two-step localization methods are often suboptimal because they overlook the fundamental constraint that all location-related parameters should converge at the same source location. To overcome the drawbacks, a new localization paradigm, namely, direct position determination (DPD), is proposed to locate sources directly from the received signals without the process of parameter extraction [18], [19], [20]. The DPD paradigm demonstrates a pronounced performance advantage over its two-step counterparts, particularly under low SNR conditions.

Another challenge in practice is the model errors within the sensor network, such as time–frequency synchronization discrepancies [21], gain and phase errors [22], and uncertainties in sensor positions [23], further complicating the localization process. Leaving these errors alone leads to a marked decrease in localization accuracy. Although the DPD paradigm offers considerable advantages, similar to two-step methods, its efficacy is also significantly compromised by model errors [24]. In the literature, there is an abundance of research on two-step localization approaches that account for model errors [23], [25], [26], [27], [28], while relatively very limited results have been reported on the DPD paradigm.

A. Related Works

For the DPD paradigm in the presence of model errors, Amar and Weiss [24] derived a general model to examine

the performance of a DPD approach in presence of model errors, including multipath, sensor position uncertainty, and antenna mutual coupling, by assuming that the emitted signal waveform is known. Wang and Wu [29] analyzed the statistical performance of a DPD method based on Doppler shifts applying the matrix eigenperturbation theory and showed that model errors lead to considerable accuracy loss. Analysis of the performance of a DPD method in presence of array response model errors was conducted in [30] for an AoA-based localization scenario. Following the work in [30], Wang et al. [31] proposed an improved robustness to sensor position and velocity uncertainties by establishing an optimization model that accounts for the model errors. The optimization problem was solved using an alternating minimization approach. Yin et al. [32] considered the localization of a stationary transmitter by separated moving arrays whose precise locations and velocities are not available. Wu et al. [33] considered the problem of DPD using a single moving array in the presence of deterministic sensor gain and phase errors. An eigenstructure-based self-calibrating DPD method is introduced to reduce the localization bias caused by these errors. An alternative two-step framework is introduced to reduce computational complexity. Yin et al. [34] exploited the noncircular property of the signals and the a priori information of satellite orbit error distribution to jointly calibrate orbit errors and locate the transmitter. An alternating iteration scheme was also adopted in [34] to estimate various unknowns. The proposed algorithm was shown to be more robust to SNR and satellite orbit errors compared with conventional two-step approaches.

By accounting model errors into the DPD paradigm, it is natural to expect better localization accuracy. However, few results have been reported on DPD in presence of model errors when external calibrators are available. Wu et al. [35] proposed a two-step method for DPD with a single moving array in the presence of sensor gain and phase errors and a calibrator with known position. Yang et al. [36] addressed the problem of DPD for a stationary emitter with several arrays in the presence of sensor gain and phase errors.

B. Major Contribution

Sensor position uncertainties are a common issue in practice, yet it remains unclear whether the DPD paradigm can robustly handle model errors with the assistance of one or more calibrators. As observed and further discussed in [33], low SNR conditions often exacerbate model errors, leading to significant localization inaccuracies. To address this challenge, we have developed a two-step DPD algorithm, and the major contributions of this work include the following.

1) *Refinement of Gibbs Sampling (GS) Method:* A refined GS algorithm is developed as the initial step to effectively tackle the sensor positions calibration problem using the calibration signal. This method is designed to manage the complexities associated with high-dimensional optimization efficiently.

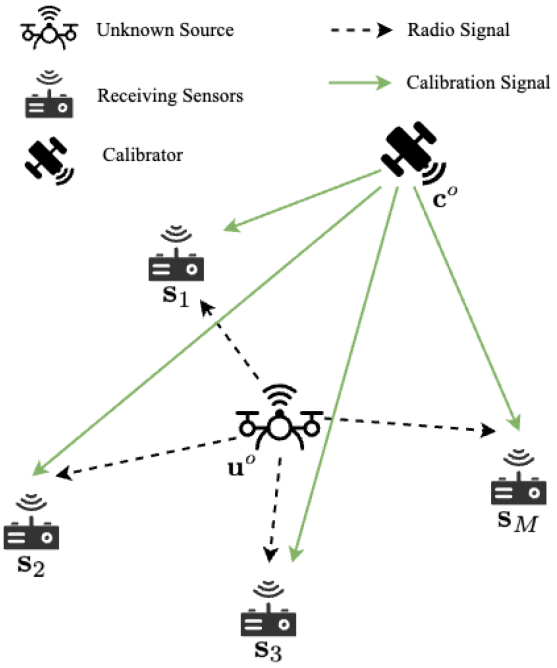

Fig. 1. Illustration of the localization scenario.

2) *Emitter Position Determination:* In the second step, we estimate the emitter's position, taking into account not only the measurement noises but also the residual uncertainties in the sensor's position. To better handle these uncertainties, especially under conditions of low SNR and high sensor position uncertainty, we introduce a revised DPD formulation based on the calibrated sensor positions. This new formulation is demonstrated to be more robust to sensor position uncertainty compared to existing methods.
3) *Performance Validation:* Monte Carlo simulations are carried out for performance evaluation, indicating that our algorithm performs superiorly compared to several benchmarks and approaches the Cramer–Rao lower bound (CRLB) under reasonable SNRs and sensor position uncertainty levels.

The rest of this article is organized as follows. Section II introduces the measurement models along with the relevant symbols and notations. Section III discusses basic emitter localization techniques that do not utilize a calibration signal, indicating the impact of sensor position uncertainty. In Section IV, the developed DPD algorithm for emitter localization is presented, and Section V conducts various numerical simulations to evaluate the performance of the proposed algorithm. Finally, Section VI concludes this article.

II. SYSTEM MODEL

Consider a 3-D localization scenario, as illustrated in Fig. 1, where a total of M receiving sensors are involved. The original positions of these sensors are denoted by $\mathbf{s}_i^o = [x_{\mathrm{s},i}^o, y_{\mathrm{s},i}^o, z_{\mathrm{s},i}^o]^T$ for $i = 1, 2, \ldots, M$. However, due to various

factors, such as deployment imprecision, the exact sensor positions are not known [23]. The available position $\mathbf{s}_i$ is a noisy version of the true position $\mathbf{s}_i^o$, modeled as

$$\mathbf{s}_i^o = \mathbf{s}_i + \mathbf{\Delta}_i, \quad i = 1, 2, \ldots, M$$

where $\mathbf{\Delta}_i$ is the ith sensor's position error. Compactly, the available sensor position is collected as

$$\mathbf{s}^o = \mathbf{s} + \mathbf{\Delta} \tag{1}$$

where $\mathbf{s}^o=[\mathbf{s}_1^{oT}, \mathbf{s}_2^{oT}, \ldots, \mathbf{s}_M^{oT}]^T$, $\mathbf{\Delta}=[\mathbf{\Delta}_1^T, \mathbf{\Delta}_2^T, \ldots, \mathbf{\Delta}_M^T]^T$, and $\mathbf{\Delta}$ is assumed to be a zero mean Gaussian vector with the covariance matrix $\mathbf{Q}_s = \sigma_s^2\mathbf{I}_{3M}$. In this scenario, the sensors are tasked with localizing a stationary source located at an unknown position $\mathbf{u}^o = [x_u^o, y_u^o, z_u^o]^T$. In this work, we consider utilizing a calibration unit to managing the uncertainty of sensor positions. This unit is strategically placed at a well-defined location $\mathbf{c}^o = [x_c^o, y_c^o, z_c^o]^T$ and transmits calibration signal that is captured by the sensors, which is used to refine the estimates of the sensor positions, thereby improving the accuracy of estimating $\mathbf{u}^o$.

A. Signal Model

The calibration unit emits calibration signal $r_c(t)$ that can be received by all sensors, and the propagation time from the calibration unit to sensor i is

$$\tau_{ci} = \|\mathbf{c}^o - \mathbf{s}_i^o\|/c \tag{2}$$

where c is the speed of light. The calibration signal received by sensor i is modeled as

$$z_{ci}(t) = \eta_{ci} r_c(t - \tau_{ci}) + w_{ci}(t)$$

where η_{ci} denotes the unknown path attenuation factor from the calibration unit to sensor i, and $w_{ci}(t)$ is zero-mean and circular Gaussian noise with $\mathbb{E}\{[w_{ci}(t)]^2\} = \sigma_{ci}^2$.

Let ΔT be the sampling interval that is adopted by all sensors, then the sampled signal is $z_{ci}[n] = \eta_{ci} r_c(n\Delta T + t_0 - \tau_{ci}) + w_{ci}[n]$, where $w_{ci}[n] = w_{ci}(n\Delta T + t_0)$, and t_0 is the initial moment of signal sampling. Suppose a total of N_c points are sampled, then the collected calibration signal vector is

$$\mathbf{z}_{ci} = [z_{ci}[0], z_{ci}[1], \ldots, z_{ci}[N_c - 1]]^T$$

and similarly, denote signal vectors $\mathbf{r}_c$ and $\mathbf{w}_{ci}$ as

$$\mathbf{r}_c = [r_c[0], \ldots, r_c[N_c - 1]]^T,$$
$$\mathbf{w}_{ci} = [w_{ci}[0], \ldots, w_{ci}[N_c - 1]]^T$$

where $\mathbf{r}_c$ is considered to be uncorrelated, i.e., $\mathbb{E}[\mathbf{r}_c\mathbf{r}_c^H] = \mathbf{I}_{N_c}$.

For convenience of further derivation, it is necessary to represent $\mathbf{z}_{ci}$ in terms of $\mathbf{r}_c$. Following the discrete Fourier transform trick [18], [19], $\mathbf{z}_{ci}$ can be derived as

$$\mathbf{z}_{ci} = \eta_{ci} \underbrace{\mathbf{F}_c^H \mathbf{D}_{\tau_{ci}} \mathbf{F}_c}_{\mathbf{Q}_{ci}} \mathbf{r}_c + \mathbf{w}_{ci} = \eta_{ci}\mathbf{Q}_{ci}\mathbf{r}_c + \mathbf{w}_{ci} \tag{3}$$

where

$$\mathbf{F}_c = \frac{1}{\sqrt{N_c}} \exp\left(-j\frac{2\pi}{N_c}\bar{\mathbf{n}}_c\bar{\mathbf{n}}_c^T\right),$$
$$\bar{\mathbf{n}}_c = \left[-\frac{N_c}{2}, \ldots \frac{N_c}{2} - 1\right]^T$$
$$\mathbf{D}_{\tau_{ci}} = \text{diag}\left\{\exp\left(-j\frac{2\pi}{N_c}\mathbf{n}_c\frac{\tau_{ci}}{\Delta T}\right)\right\},$$
$$\mathbf{n}_c = [0, 1, \ldots, N_c - 1]^T.$$

For the emitter, its emitted unknown source signal received by sensor i can be modeled as

$$z_i(t) = \eta_i r(t - \tau_i) + w_i(t)$$

where η_i is the path attenuation factor from the emitter to sensor i, $w_i(t)$ is zero-mean and independent circular Gaussian noise with $\mathbb{E}\{w_i^2(t)\} = \sigma_i^2$, and τ_i is the propagation delay with

$$\tau_i = \|\mathbf{u}^o - \mathbf{s}_i^o\|/c.$$

Suppose a total of N points of the received signal are sampled, then the collected signal vector is

$$\mathbf{z}_i = [z_i[0], z_i[1], \ldots, z_i[N - 1]]^T$$

and similarly, denote signal vectors $\mathbf{r}$ and $\mathbf{w}_i$ as

$$\mathbf{r} = [r[0], \ldots, r[N - 1]]^T, \ \mathbf{w}_i = [w_i[0], \ldots, w_i[N - 1]]^T$$

where $\mathbf{r}$ is considered to be uncorrelated, i.e., $\mathbb{E}[\mathbf{r}\mathbf{r}^H] = \mathbf{I}_N$. Thus, $\mathbf{z}_i$ can be modeled as

$$\mathbf{z}_i = \eta_i \underbrace{\mathbf{F}^H \mathbf{D}_{\tau_i} \mathbf{F}}_{\mathbf{Q}_i} \mathbf{r} + \mathbf{w}_i = \eta_i \mathbf{Q}_i \mathbf{r} + \mathbf{w}_i \tag{4}$$

where

$$\mathbf{F} = \frac{1}{\sqrt{N}} \exp\left(-j\frac{2\pi}{N}\bar{\mathbf{n}}\bar{\mathbf{n}}^T\right), \ \bar{\mathbf{n}} = \left[-\frac{N}{2}, \ldots, \frac{N}{2} - 1\right]^T$$
$$\mathbf{D}_{\tau_i} = \text{diag}\left\{\exp\left(-j\frac{2\pi}{N}\mathbf{n}\frac{\tau_i}{\Delta T}\right)\right\}, \ \mathbf{n} = [0, 1, \ldots, N - 1]^T.$$

By collecting signal from all sensors, calibration signal samples $\{\mathbf{z}_{ci}\}_{i=1}^M$ are collected as

$$\mathbf{z}_c = \boldsymbol{\eta}_c\mathbf{Q}_c\mathbf{r}_c + \mathbf{w}_c \tag{5}$$

where

$$\mathbf{z}_c = \left[\mathbf{z}_{c1}^T, \ldots, \mathbf{z}_{cM}^T\right]^T, \ \mathbf{w}_c = \left[\mathbf{w}_{c1}^T, \ldots, \mathbf{w}_{cM}^T\right]^T$$
$$\mathbf{Q}_c = \left[\mathbf{Q}_{c1}^T, \ldots, \mathbf{Q}_{cM}^T\right]^T, \ \boldsymbol{\eta}_c = \text{diag}\left(\eta_{c1}, \ldots, \eta_{cM}\right) \otimes \mathbf{I}_{N_c}$$

and $\mathbf{w}_c$ is also a zero-mean Gaussian noise with covariance

$$\text{Cov}\{\mathbf{w}_c\} = \mathbf{\Lambda}_c = \text{blkdiag}\left\{\sigma_{c1}^2\mathbf{I}_{N_c}, \sigma_{c2}^2\mathbf{I}_{N_c}, \ldots, \sigma_{cM}^2\mathbf{I}_{N_c}\right\}.$$

Similarly, the received signal samples $\{\mathbf{z}_i\}_{i=1}^M$ can be compactly modeled as

$$\mathbf{z} = \boldsymbol{\eta}\mathbf{Q}\mathbf{r} + \mathbf{w} \tag{6}$$

where

$$\mathbf{z} = \left[\mathbf{z}_1^T, \ldots, \mathbf{z}_M^T\right]^T, \ \mathbf{w} = \left[\mathbf{w}_1^T, \ldots, \mathbf{w}_M^T\right]^T$$
$$\mathbf{Q} = \left[\mathbf{Q}_1^T, \ldots, \mathbf{Q}_M^T\right]^T, \ \boldsymbol{\eta} = \text{diag}\left(\eta_1, \ldots, \eta_M\right) \otimes \mathbf{I}_N$$

and $\mathbf{w}$ is a zero-mean Gaussian noise with covariance

$$\text{Cov}\{\mathbf{w}\} = \mathbf{\Lambda} = \text{blkdiag}\left\{\sigma_1^2\mathbf{I}_N, \sigma_2^2\mathbf{I}_N, \ldots, \sigma_M^2\mathbf{I}_N\right\}.$$

Given measurements $\mathbf{s}$ in (1), $\mathbf{z}_c$ in (5), and $\mathbf{z}$ in (6), our goal is to estimate source location $\mathbf{u}^o$ and sensor positions $\mathbf{s}^o$. Next, we first investigate the case without a calibrator and present a revised DPD method that accounts for the sensor position uncertainty in Section III. Our findings highlight the importance of considering the sensor position uncertainty. Subsequently, in Section IV, we incorporate the calibrator and develop a calibration signal-assisted DPD method.

III. DPD WITHOUT CALIBRATOR

Consider there is no calibrator whereas only signal sample vector $\mathbf{z}$ is accessible. In such a case, a simplistic approach to estimate $\mathbf{u}^o$ might overlook sensor position errors and thus the standard DPD method could be applied. However, this approach fails to leverage the valuable insights that sensor position errors tend to be minor and that there is covariance information available regarding these errors. In the next, a revised DPD method that accounts the sensor position uncertainty will be developed.

Since matrix $\mathbf{Q}$ in (6) can be regarded as a nonlinear function w.r.t. $\mathbf{u}^o$ and $\mathbf{s}^o$, i.e., $\mathbf{Q} = \mathbf{Q}(\mathbf{u}^o, \mathbf{s}^o)$, then applying the first-order Taylor-series expansion, we have the following re-expression for $\mathbf{z}$.

PROPOSITION 1 Let $\mathbf{s}^o = \mathbf{s} + \mathbf{\Delta}$ and $\mathbf{z}$ be defined in (6). Then, by applying the first-order Taylor-series expansion of $\mathbf{z}$ w.r.t. $\mathbf{s}^o$ at $\mathbf{s}$, $\mathbf{z}$ can be re-expressed as

$$\mathbf{z} = \boldsymbol{\eta}\mathbf{Q}(\mathbf{u}^o, \mathbf{s})\mathbf{r} + \mathbf{v} + o(\|\mathbf{\Delta}\|^2)$$

where

$$\mathbf{v} = \frac{\partial \boldsymbol{\eta}\mathbf{Q}(\mathbf{u}^o, \mathbf{s}^o)\mathbf{r}}{\partial \mathbf{s}^o}|_{\mathbf{s}^o=\mathbf{s}}\mathbf{\Delta} + \mathbf{w}$$

is a circular Gaussian noise with $\mathbb{E}\{\mathbf{v}\} = \mathbf{0}$. Further, the covariance of $\mathbf{v}$ can be approximated as

$$\text{Cov}\{\mathbf{v}\} = \mathbf{\Lambda}_v \approx \text{blkdiag}\left\{\varrho_1^2\mathbf{I}_N, \varrho_2^2\mathbf{I}_N, \ldots, \varrho_M^2\mathbf{I}_N\right\}$$

where

$$\varrho_i^2 = \sigma_i^2 + \alpha\hat{P}_i\left(\frac{2\pi}{N\Delta Tc}\right)^2\sigma_s^2 \quad \forall i.$$

In the above, $\alpha = \text{tr}(\mathbf{F}^H\text{diag}\{\mathbf{n}^2\}\mathbf{F})/N$, and $\hat{P}_i$ is the signal power estimated from $\mathbf{z}_i$.

The proof of Proposition 1 follows chain rule for partial derivatives, and details are presented in Appendix A. Based on Proposition 1, the maximum likelihood estimation (MLE) for $\mathbf{u}^o$ is in a weighted least square (WLS) form, given as

$$\min_{\boldsymbol{\eta},\mathbf{r},\mathbf{u}^o} \left(\mathbf{z} - \boldsymbol{\eta}\mathbf{Q}(\mathbf{u}^o, \mathbf{s})\mathbf{r}\right)^H \mathbf{\Lambda}_{\mathbf{v}}^{-1}\left(\mathbf{z} - \boldsymbol{\eta}\mathbf{Q}(\mathbf{u}^o, \mathbf{s})\mathbf{r}\right). \quad (7)$$

Problem (7) involves three types of optimization variables, i.e., $\boldsymbol{\eta}$, $\mathbf{r}$, and $\mathbf{u}^o$; direct resolution of all variables is unwarranted, given that $\mathbf{u}^o$ is the variable of interest. In addition, the specific quadratic structure of the loss function enables the development of an efficient computational approach, circumventing the need to solve for $\boldsymbol{\eta}$ and $\mathbf{r}$ explicitly. The following proposition shows that Problem (7) can be equivalently recast as a problem of finding the largest eigenvalue, where $\mathbf{u}^o$ is the only optimization variable.

PROPOSITION 2 Let $\hat{\mathbf{u}}^o$ be the optimal solution of problem (7), then it is also the optimal solution of the following problem:

$$\hat{\mathbf{u}}^o = \arg\max_{\mathbf{u}^o} \lambda_{\max}\left(\mathbf{R}\left(\mathbf{u}^o\right)\right) \quad (8)$$

where $\mathbf{R}(\mathbf{u}^o)$ is the cross-correlation matrix with its (i, j)th entity being

$$\mathbf{R}_{ij}\left(\mathbf{u}^o\right) = \frac{\mathbf{z}_i^H\mathbf{Q}_i(\mathbf{u}^o, \mathbf{s})\mathbf{Q}_j(\mathbf{u}^o, \mathbf{s})^H\mathbf{z}_j}{\varrho_i^2\varrho_j^2}. \quad (9)$$

The proof of Proposition 2 employs tricks analogous to those used in [37], with the full details provided in Appendix B. Following the grid search methodology [37], the estimate $\hat{\mathbf{u}}^o$ can be obtained.

REMARK 1 It is important to note that Problem (8) is different from the vanilla DPD algorithm since it incorporates the sensor position uncertainty, which is ultimately reflected in the computation of $\mathbf{R}(\mathbf{u}^o)$ as detailed in (9). Overlooking the sensor position uncertainty would simplify the term $\varrho_i^2\varrho_j^2$ to $\sigma_i^2\sigma_j^2$, a variation that significantly impacts localization accuracy. These implications will be illustrated in the simulations presented in Section V-A.

IV. DPD WITH CALIBRATOR

A. MLE of Sensor Positions

Considering a calibrator is available, the collected calibration signal samples $\mathbf{z}_c$ defined in (5) can be utilized to effectively estimate $\mathbf{s}^o$. Together with the prior information of sensor positions described in (1), the maximum a posterior estimation of sensor positions is

$$\min_{\boldsymbol{\eta}_c,\mathbf{r}_c,\mathbf{s}^o} \|\mathbf{z}_c - \boldsymbol{\eta}_c\mathbf{Q}_c(\mathbf{s}^o)\mathbf{r}_c\|^2_{\mathbf{\Lambda}_c^{-1}} + \frac{1}{\sigma_s^2}\|\mathbf{s}^o - \mathbf{s}\|^2 \quad (10)$$

where $\mathbf{\Lambda}_c = \text{diag}\{\sigma_{c1}^2, \sigma_{c2}^2, \ldots, \sigma_{cM}^2\}$. Problem (10) can be reformulated as a regularized problem of finding the largest eigenvalue, given in the following proposition.

PROPOSITION 3 Let $\hat{\mathbf{s}}^o$ be the optimal solution of Problem (10), then it is also the optimal solution of the following problem:

$$\hat{\mathbf{s}}^o = \arg\max_{\mathbf{s}^o} \lambda_{\max}\{\mathbf{R}_c(\mathbf{s}^o)\} - \frac{1}{\sigma_s^2}\|\mathbf{s}^o - \mathbf{s}\|^2 \quad (11)$$

where $\mathbf{R}_c(\mathbf{s}^o)$ is the cross-correlation matrix with its (i, j)th entity being

$$R_{cij}(\mathbf{s}^o) = \frac{\mathbf{z}_{ci}^H\mathbf{Q}_{ci}(\mathbf{s}^o)\mathbf{Q}_{cj}(\mathbf{s}^o)^H\mathbf{z}_{cj}}{\sigma_{ci}^2\sigma_{cj}^2}. \quad (12)$$

The tricks of proving Proposition 3 are similar to those used in Proposition 2, with details omitted here. It is important to recognize that Problem (11) is considerably more challenging than Problem (8). The vector $\mathbf{s}^o$ has a dimension

of $3M$, whereas $\mathbf{u}^o$ is only 3-D, leading to a grid search for $\mathbf{s}^o$ that is computationally demanding.

B. Refined GS

To address Problem (11), a refined version of GS is employed, which is an efficient sampling method for statistical inference [38]. Given the need to perform a computationally intensive grid search over a parameter space of dimension $3M$, GS can efficiently generate samples from high-dimensional probability distributions through sequential sampling. This method aligns the distribution's mode with the optimization problem's optima, thereby approximating the optimal solution after a sufficient number of iterations.

1) *Vanilla GS Procedure:* In applying GS to solve Problem (11), the potential sensor position space is discretized into a grid of finely partitioned cubic regions. For each sensor i, the search region $\mathcal{S}_i$ is divided into a cubic grid centered at initial position $\mathbf{s}_i$, this region is uniformly partitioned along the X-, Y-, and Z-axes. Each axis extends over a length of $3\sigma_s$ and the grid comprises N_g points along each axis. At the nth iteration, the sample is denoted as $S^n = (\mathbf{s}_1^n, \mathbf{s}_2^n, \ldots, \mathbf{s}_M^n)$, where $\mathbf{s}_i^n \in \mathcal{S}_i$ for each sensor i. The entire sample space is the product space $\mathcal{S} = \mathcal{S}_1 \times \mathcal{S}_2 \times \ldots \times \mathcal{S}_M$. To ensure the Markov chain properties across the samples $S^1, S^2, \ldots$, we introduce M subiterations within each main iteration n. In each subiteration, we update the position of one sensor, holding the positions of all other sensors constant. This sequential updating scheme facilitates the convergence of the Markov chain to the distribution of interest, yielding an effective method for approaching the optimal solution to Problem (11). In particular, denote $S_i^n = (\mathbf{s}_1^n, \ldots, \mathbf{s}_i^n, \mathbf{s}_{i+1}^{n-1}, \ldots, \mathbf{s}_M^{n-1})$, the evolution of the Markov chain is depicted as

$$S_1^1 \to \cdots \to S_{M-1}^n \to S_M^n \to S_1^{n+1} \to S_2^{n+1} \to \cdots \quad (13)$$

where $\to$ represents a single subiteration that the position of one sensor is updated, and with the convention that $S^n = S_M^n$ represents the complete sample vector after all M sensors have been updated in the nth iteration. For this GS procedure to successfully resolve Problem (11), it is critical to carefully design the state transition probability $\mathbb{P}(S_m^n \mid S_{m-1}^n)$. This probability must be crafted to ensure that each subiteration promotes movement toward the high-probability regions of the solution space, allowing the GS algorithm to converge to an approximation close to the optimal solution. Specifically, denote $S_{-i}^n = (\mathbf{s}_1^n, \ldots, \mathbf{s}_{i-1}^n, \mathbf{s}_{i+1}^{n-1}, \ldots, \mathbf{s}_M^{n-1})$ as a sample at iteration n excluding the position of the ith sensor, and define $S_{-i}^n \wedge \mathbf{s} = (\mathbf{s}_1^n, \ldots, \mathbf{s}_{i-1}^n, \mathbf{s}, \mathbf{s}_{i+1}^{n-1}, \ldots, \mathbf{s}_M^{n-1})$, which combines with a potential new position $\mathbf{s}$ for sensor i. With relation $S_i^n = S_{-i}^n \wedge \mathbf{s}_i^n$ and $S_{i-1}^n = S_{-i}^n \wedge \mathbf{s}_i^{n-1}$, the state transition probability associating with Problem (11) is defined as

$$\mathbb{P}\left(S_i^n \mid S_{i-1}^n\right) = \mathbb{P}\left(S_{-i}^n \wedge \mathbf{s}_i^n \mid S_{-i}^n \wedge \mathbf{s}_i^{n-1}\right)$$

$$= \frac{e^{\mu g(S_{-i}^n \wedge \mathbf{s}_i^n)}}{\sum_{\mathbf{s}\in\mathcal{S}_i} e^{\mu g(S_{-i}^n \wedge \mathbf{s})}} := \mathbb{P}_i^n(\mathbf{s}_i^n) \quad \forall \mathbf{s}_i^n \in \mathcal{S}_i \quad (14)$$

where $\mu > 0$ is a predetermined parameter and

$$g(S^n) = \lambda_{\max}\{\mathbf{R}_c(S^n)\} - \frac{1}{\sigma_s^2}\|S^n - \mathbf{s}\|^2.$$

During the ith subiteration of the nth iteration, the position $\mathbf{s}_i^n$ is sampled according to the probability distribution specified in (14). This probabilistic mechanism ensures that the sampling is biased toward configurations that maximize the loss function, progressively leading to an increasingly accurate approximation of the optimal sensor positions. An advantageous characteristic of this GS procedure is its convergence to the stationary distribution of the Markov chain (13). This stationary distribution can be described as

$$\lim_{n\to\infty} \mathbb{P}(S^n = S) = \frac{e^{\mu g(S)}}{\sum_{S'\in\mathcal{S}} e^{\mu g(S')}} := \Pi(S) \quad \forall S \in \mathcal{S}.$$

As the parameter μ approaches infinity, the stationary distribution $\Pi(S)$ for the optimal solution $S = \hat{\mathbf{s}}^o$ to Problem (11) approaches 1. Consequently, for a sufficiently large number of iterations n, S^n can be considered as an approximate optimal solution to Problem (11). The quality of this approximation is influenced by two main factors: the discrete nature of the position set $\mathcal{P}$, and the fact that in practice, the value of μ is finite. It is important to note that a larger μ can result in slower convergence of the GS procedure, whereas a smaller μ may yield a larger optimality gap. This gap is theoretically upper bounded by $1/\mu$ [38]. Therefore, selecting the value of μ is a tradeoff between computational efficiency and the performance gap. This tradeoff will be explored numerically in the simulations presented in Section V-B.

2) *Refined GS Procedure:* In addition, calculating the state transition probabilities as specified in (14) necessitates solving the largest eigenvalue problem $|\mathcal{S}_i|$ times at each subiteration, which could be computationally intensive. To improve the efficiency of the GS procedure, we propose a refinement that partitions $\mathcal{S}_i$ into two disjointed subsets $\mathcal{S}_{Li}^n$ and $\mathcal{S}_{Ri}^n$, depending on the current iteration n. During the ith subiteration of the nth iteration, $\mathcal{S}_{Li}^n$ encompasses the current position $\mathbf{s}_i^{n-1}$, as well as its immediately nearby positions, effectively allowing a localized search within the immediate vicinity for potential improvements. This set is chosen to facilitate swift evaluation of neighboring positions that may yield incremental enhancements to the solution. Conversely, $\mathcal{S}_{Ri}^n$ is constructed by randomly selecting κ positions from $\mathcal{S}_i$ excluding $\mathcal{S}_{Li}^n$, where κ is significantly smaller than $|\mathcal{S}_i|$. This set is intended to sample diverse positions from across the entire state space, providing a mechanism to escape local optima by considering solutions that may not be in the immediate neighborhood of the current position. By using $\mathcal{S}_{Li}^n$ for rapid local explorations and $\mathcal{S}_{Ri}^n$ for global search, the GS procedure achieves a balance between exploitation of the known good areas of the solution space and exploration of new areas that might offer better solutions. This approach

helps to enhance the convergence speed and the quality of the final solution while mitigating the computational burden associated with the eigenvalue problem that needs to be solved at each subiteration.

Finally, the proposed GS procedure for solving Problem (11) is summarized below.

1) *Initialization:* Selecting a well-informed initial state S^1 is beneficial to expedite the iteration process of the proposed GS procedure. Given that calibration signals are reliably received by all sensors, the TDOA can be readily determined. Consequently, we choose to employ the linear minimum mean square error (LMMSE) estimator of $\mathbf{s}^o$ predicated on range differences of arrival [3] to initialize S^1.
2) *Sampling iteration:* In accordance with the Markov chain in (13), we determine the position $\mathbf{s}_i^n$ for the ith sensor during the nth iteration's subiteration based on the probability distribution outlined in (14). In particular, the set $\mathcal{S}_i$ referenced in (14) is partitioned into two subsets: $\mathcal{S}_{Li}^n$ and $\mathcal{S}_{Ri}^n$. Rather than drawing $\mathbf{s}_i^n$ directly from the probability distribution $\mathbb{P}_i^n(\cdot)$ or adopting a maximum a posteriori criterion policy, we construct $\mathbf{s}_i^n$ using the expected a posteriori policy. This policy effectively selects the mean of all possible positions weighted by their respective posterior probabilities, which is estimated as $\mathbf{s}_i^n = \sum_{\mathbf{s}_i \in \mathcal{S}_i} \mathbb{P}_i^n(\mathbf{s}_i)\mathbf{s}_i$, and the estimated position $\mathbf{s}_i^n$ would be rounded to the corresponding nearest grid point. As opposed to selecting the single probable position as in the maximum a posteriori policy, incorporating information from the entire probability distribution potentially leads to a more robust estimate that accounts for the uncertainty in the sensor positions.
3) *Stopping criterion:* The sampling iteration is repeated until the sensor positions converge or the iteration stopping criterion is satisfied. The iteration stopping criterion could be the iteration number or a distance criterion $\|S^n - S^{n-1}\| \leq \delta$, where $\delta > 0$ is a small threshold. After the iteration stops, we obtain the solution

$$\bar{\mathbf{s}}^o = S^{N_{\text{iter}}} \tag{15}$$

where N_{iter} is the number of iterations.

C. Direct Position Determination

Let $\bar{\mathbf{s}}^o$ be given by (15), then similar to Proposition 1, $\mathbf{z}$ in (6) can be re-expressed as the following.

PROPOSITION 4 Let $\mathbf{s}^o = \bar{\mathbf{s}}^o + \Delta\bar{\mathbf{s}}^o$ and $\mathbf{z}$ be defined in (6). Then, by applying the first-order Taylor-series expansion of $\mathbf{z}$ w.r.t. $\mathbf{s}^o$ at $\bar{\mathbf{s}}^o$, $\mathbf{z}$ can be re-expressed as

$$\mathbf{z} = \boldsymbol{\eta}\mathbf{Q}(\mathbf{u}^o, \bar{\mathbf{s}}^o)\mathbf{r} + \bar{\mathbf{v}} + o\left(\|\Delta\bar{\mathbf{s}}^o\|^2\right)$$

where

$$\bar{\mathbf{v}} = \frac{\partial \boldsymbol{\eta}\mathbf{Q}(\mathbf{u}^o, \mathbf{s}^o)\mathbf{r}}{\partial \mathbf{s}^o}\Big|_{\mathbf{s}^o=\bar{\mathbf{s}}^o} \Delta\bar{\mathbf{s}}^o + \mathbf{w}$$

is the noise depending on the estimator $\bar{\mathbf{s}}^o$.

The main distinction between Propositions 1 and 4 lies in the selection of the sensor position used as the reference point for the Taylor-series expansion. Specifically, Proposition 1 performs the Taylor-series expansion at the available position $\mathbf{s}$ characterized in (1), while Proposition 4 performs the expansion at the estimated position $\bar{\mathbf{s}}^o$, which is estimated from $\mathbf{s}$ and the calibration signal $\mathbf{z}_c$. Inclusion of the calibration signal $\mathbf{z}_c$ diminishes the uncertainty associated with the sensor position, thereby enhancing the localization accuracy for $\mathbf{u}^o$. It is important to recognize that $\bar{\mathbf{s}}^o$ represents a computationally feasible numerical solution for the MLE $\hat{\mathbf{s}}^o$ defined in (10). Provided that $\bar{\mathbf{s}}^o$ is in close proximity to $\hat{\mathbf{s}}^o$, that is, $\hat{\mathbf{s}}^o \approx \bar{\mathbf{s}}^o$, we can invoke the asymptotic normality of the MLE to approximate that $\mathbb{E}\{\bar{\mathbf{v}}\} \approx \mathbf{0}$. Based on this approximation, the covariance of $\bar{\mathbf{v}}$ becomes useful for establishing a WLS estimator to later estimate $\mathbf{u}^o$. The following proposition provides an approximation for the covariance of $\bar{\mathbf{v}}$.

PROPOSITION 5 The covariance of $\bar{\mathbf{v}}$ can be approximated in a block diagonal form as

$$\text{Cov}\{\bar{\mathbf{v}}\} = \boldsymbol{\Lambda}_{\bar{\mathbf{v}}} \approx \text{blkdiag}\left\{\bar{\varrho}_1^2\mathbf{I}_N, \bar{\varrho}_2^2\mathbf{I}_N, \ldots, \bar{\varrho}_M^2\mathbf{I}_N\right\} \tag{16}$$

where

$$\bar{\varrho}_i = \sigma_i^2 + \left(\frac{3\sigma_s^2 + 2\alpha_{ci}\hat{P}_{ci}\sigma_s^4}{3 + \alpha_{ci}\hat{P}_{ci}\sigma_s^2}\hat{P}_i\left(\frac{2\pi}{N\Delta T c}\right)^2\right) \quad \forall i.$$

In the above, $\hat{P}_i$ and $\hat{P}_{ci}$ are the signal power estimated from $\mathbf{z}_i$ and $\mathbf{z}_{ci}$, respectively, and

$$\alpha_{ci} = \frac{\text{tr}\left(\mathbf{F}_c^H \text{diag}\left\{\mathbf{n}_c{}^2\right\}\mathbf{F}_c\right)}{N_c}\left(\left(\frac{2\pi}{N_c\Delta T c}\right)^2\sigma_{ci}^{-2}\right).$$

The proof of Proposition 5 is presented in Appendix C.

REMARK 2 Note that $\bar{\varrho}_i$ differs from ϱ_i as presented in Proposition 1. This difference arises because $\bar{\varrho}_i$ includes the effects of using $\mathbf{z}_{ci}$ in the estimation of $\mathbf{s}_i^o$.

Based on Propositions 4 and 5, a WLS estimator is proposed to estimate $\mathbf{u}^o$, given as

$$\min_{\boldsymbol{\eta},\mathbf{r},\mathbf{u}^o} \left(\mathbf{z} - \boldsymbol{\eta}\mathbf{Q}(\mathbf{u}^o, \bar{\mathbf{s}}^o)\mathbf{r}\right)^H \boldsymbol{\Lambda}_{\bar{\mathbf{v}}}^{-1}\left(\mathbf{z} - \boldsymbol{\eta}\mathbf{Q}(\mathbf{u}^o, \bar{\mathbf{s}}^o)\mathbf{r}\right). \tag{17}$$

Similar to Proposition 2, Problem (17) can be equivalently recast as a problem of finding the largest eigenvalue with $\mathbf{u}^o$ being the only optimization variable.

PROPOSITION 6 Let $\hat{\mathbf{u}}^o$ be the optimal solution of problem (17), then it is also the optimal solution of the following problem:

$$\hat{\mathbf{u}}^o = \arg\max_{\mathbf{u}^o} \lambda_{\max}\left(\bar{\mathbf{R}}\left(\mathbf{u}^o\right)\right) \tag{18}$$

where $\bar{\mathbf{R}}(\mathbf{u}^o)$ is the cross-correlation matrix with its (i, j)th entity being

$$\tilde{\mathbf{R}}_{ij}\left(\mathbf{u}^o\right) = \frac{\mathbf{z}_i^H\mathbf{Q}_i(\mathbf{u}^o, \bar{\mathbf{s}}^o)\mathbf{Q}_j(\mathbf{u}^o, \bar{\mathbf{s}}^o)^H\mathbf{z}_j}{\bar{\varrho}_i^2\bar{\varrho}_j^2}. \tag{19}$$

The entire procedure of the proposed DPD algorithm is summarized in Algorithm 1. It should be highlighted that $\bar{\mathbf{s}}^o$

Algorithm 1: Proposed two-step DPD algorithm.

1: Use refined GS procedure to calibrate $\bar{\mathbf{s}}^o$ by (15);
2: Calculating $\mathbf{\Lambda}_{\tilde{\mathbf{w}}}$ by (16);
3: Estimate $\hat{\mathbf{u}}^o$ by solving Problem (18).

involves in the estimation of the covariance of $\tilde{\mathbf{w}}$, making Algorithm 1 being robust to sensor position error as will be demonstrated in Section V later. Finally, the CRLB on the estimation of the emitter position $\mathbf{u}^o$, both without and with the presence of a calibrator, are provided in Appendix D.

V. NUMERICAL RESULTS

This section presents numerical simulations to evaluate the performance of the proposed algorithms. We first evaluate the performance of DPD without calibrators. Subsequently, the influence of the hyperparameter μ and the iteration number on the performance of DPD is investigated. Through this investigation, appropriate choices of μ and the iteration number are determined and use in subsequent evaluations. Following this, the performance of proposed algorithms are compared with several benchmarks. And lastly, we contrast the proposed DPD algorithm with an alternative approach that the sensor positions are treated as deterministic and optimized jointly with the emitter position.

A scenario with one emitter and $M = 4$ sensors is considered. The emitter's position is $\mathbf{u}^o = [-1, 70, 10]^T$ km and the sensor positions are $\mathbf{s}_1^o = [100, 20, 10]^T$ km, $\mathbf{s}_2^o = [50, 10, 10]^T$ km, $\mathbf{s}_3^o = [0, 0, 10]^T$ km, and $\mathbf{s}_4^o = [-30, 30, 10]^T$ km, respectively. The emitter emits binary phase-shift keying modulation signal with a bandwidth of 25 kHz. The carrier frequency is 303 MHz and the sampling rate is 100 kHz. For each trail, $N = 2000$ points are sampled for emitter localization. The received signal amplitude is inversely proportional to the distance between the emitter and a receiver, which is widely recognized in free space propagation. The position of the calibrator is set to be $\mathbf{c}^o = [10, 90, 10]^T$ km and the grid number N_g is set to be 15. The settings for the calibration signal are the same as the emitter's signal except that they have totally different source codes. The root-mean-square localization errors (RMSE) averaged over 100 independent trails are utilized as the performance metric.

A. DPD Without Calibrator

This section considers the case that no calibrator is available. The SNR of the received signals by receiver 1 ranges from -10 to 15 dB with a step size of 5 dB, and the covariance of sensor position error is set to be equal to the range difference of arrival (RDOA) covariance between sensor 1 and sensor 2 under each SNR [3]. The DPD algorithm derived in Section III, which considers the sensor position uncertainty (denoted by $\texttt{DPD}_{\texttt{NCU}}$), is evaluated. In comparison, the algorithm that simply ignores the sensor position error (denoted by $\texttt{DPD}_{\texttt{NCNU}}$) is adopted as a baseline. As depicted in Fig. 2, the rms localization error of $\texttt{DPD}_{\texttt{NCU}}$ approaches CRLB with increasing SNR. Moreover, $\texttt{DPD}_{\texttt{NCU}}$ demonstrates superior performance by yielding lower localization errors than $\texttt{DPD}_{\texttt{NCNU}}$, emphasizing the significance of accounting for sensor position uncertainty.

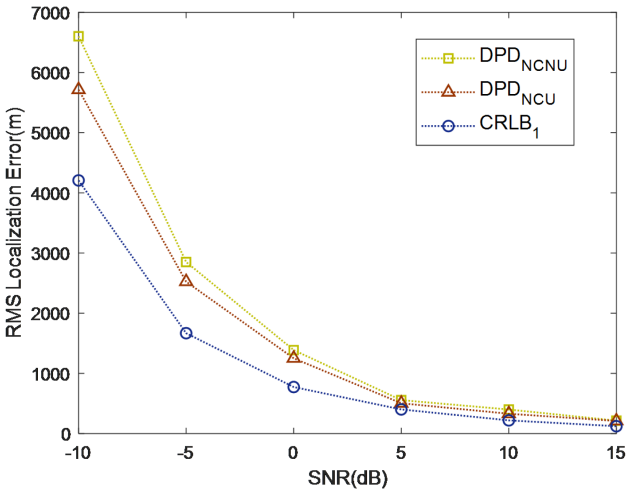

Fig. 2. RMSE of DPD without calibrator for different SNRs.

TABLE I
RMSE With Different Choice of μ and N_{iter}

N_{iter} \ μ	1	10	100	1000	2000	3000
3	1355.0	1352.6	1259.9	1021.1	947.7	870.1
5	1354.7	1349.2	1192.8	935.0	835.0	830.5
10	1353.9	1316.0	1154.0	833.4	829.6	829.2
20	1352.1	1268.9	1004.1	830.3	830.1	829.7
30	1350.6	1224.7	965.0	830.5	830.2	829.9

B. Impact of Hyperparameter and Iterations

This section evaluates the performance of DPD with different choice of μ and N_{iter}. In this evaluation, the SNRs of both the emitter's signal and the calibrator's signal received by receiver 1 are set to be -5 dB. Table I summarizes the rms localization error averaged over 100 independent trails for each choice of μ and N_{iter}. According to the results in Table I, careful adjustment of μ and N_{iter} is crucial for obtaining accurate localization estimates. For the remainder of this article, we will use $\mu = 3000$ and $N_{\text{iter}} = 5$. This configuration requires the fewest iteration runs while still delivering reasonably good performance.

C. DPD With Calibrator

This section compares the performance of the proposed DPD with several benchmarks, including: $\texttt{DPD}_{\texttt{1CU}}$ that estimates $\bar{\mathbf{s}}^o$ only using the LMMSE algorithm [3] and considers the estimation uncertainty, $\texttt{DPD}_{\texttt{1CNU}}$ that estimates $\bar{\mathbf{s}}^o$ only using the LMMSE algorithm but simply ignores the sensor position estimation uncertainty, $\texttt{DPD}_{\texttt{2CNU}}$ that estimates the $\bar{\mathbf{s}}^o$ using the refined GS algorithm but simply ignores the sensor position estimation uncertainty, $\texttt{DPD}_{\texttt{2CU}}$ that considers the estimation uncertainty, $\texttt{TS}_{\texttt{P}}$ that locates the emitter with the traditional TDOA-based two-step method with known sensor positions, $\texttt{TS}_{\texttt{1C}}$ that takes the sensor position

TABLE II
Computational Complexity of $\mathrm{DPD}_{2\mathrm{CU}}$ and $\mathrm{TS}_{1\mathrm{C}}$

Method	Complexity
$\mathrm{TS}_{1\mathrm{C}}$	$\mathcal{O}\left(2n_f n_\tau N(M-1)+2n_{f_c}n_{\tau_c}N_c(M-1)+8N_xN_yN_z(M-1)\right)$
$\mathrm{DPD}_{2\mathrm{CU}}$	$\mathcal{O}\left(2n_{f_c}n_{\tau_c}N_c(M-1)+N_xN_yN_z\left(NM+NM^2\right)+N_{\text{iter}}N_gM\left(NM+NM^2\right)\right)$

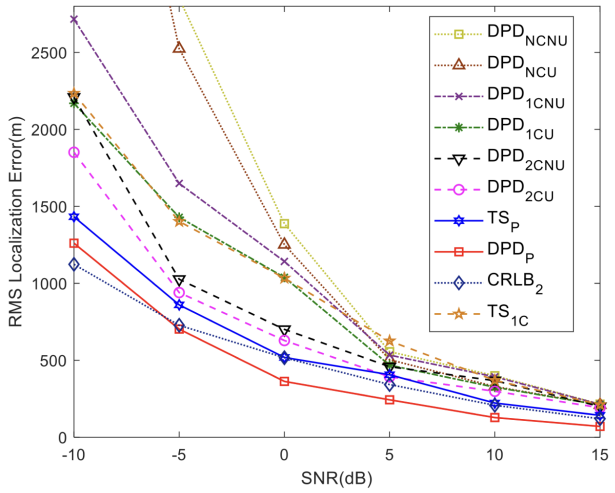

Fig. 3. RMSE of different methods for different SNRs.

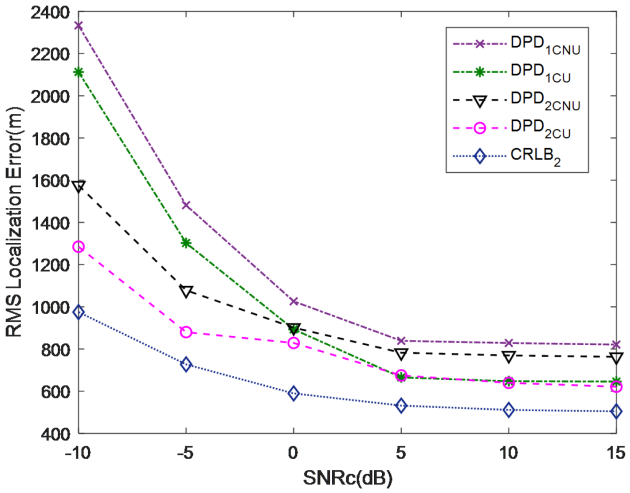

Fig. 4. RMSE of different methods for different SNRcs.

and the external calibrator into account [3], and $\mathrm{DPD}_{\mathrm{P}}$ that locates the emitter with the DPD method with known sensor positions.

We first compare the RMSE with similar setups as those in Section V-A except that a calibrator is introduced. The SNR of the calibration signals received by sensor 1 is set as -5 dB under each emitter's SNR. In Fig. 3, as expected, $\mathrm{DPD}_{\mathrm{P}}$ performs best and could even breakthrough CRLB when SNR becomes high when sensor position uncertainties are not present. On the other hand, $\mathrm{DPD}_{1\mathrm{CNU}}$, $\mathrm{DPD}_{1\mathrm{CU}}$, $\mathrm{DPD}_{2\mathrm{CNU}}$, and $\mathrm{DPD}_{2\mathrm{CU}}$ are all superior to $\mathrm{DPD}_{\mathrm{NCNU}}$ and $\mathrm{DPD}_{\mathrm{NCU}}$, demonstrating the advantage of introducing a calibrator. It can be observed that $\mathrm{DPD}_{1\mathrm{CU}}$ outperforms $\mathrm{DPD}_{1\mathrm{CNU}}$, while $\mathrm{DPD}_{2\mathrm{CU}}$ outperforms $\mathrm{DPD}_{2\mathrm{CNU}}$. Such results further highlight the importance of considering the sensor position uncertainty. The proposed $\mathrm{DPD}_{2\mathrm{CU}}$ performs best among $\mathrm{DPD}_{1\mathrm{CNU}}$, $\mathrm{DPD}_{1\mathrm{CU}}$, $\mathrm{DPD}_{2\mathrm{CNU}}$, and $\mathrm{DPD}_{2\mathrm{CU}}$, and its performance approaches CRLB when SNR becomes high, and this shows the effectiveness of the direct calibration process. Note $\mathrm{TS}_{1\mathrm{C}}$ is one state-of-the-art two-step approach, which takes the sensor position and the external calibrator into account. The proposed method $\mathrm{DPD}_{2\mathrm{CU}}$ outperforms $\mathrm{TS}_{1\mathrm{C}}$ with a significant margin when SNR is low. This verifies that the DPD scheme can effectively push a better performance than the two-step approach. The performance gap between $\mathrm{DPD}_{2\mathrm{CU}}$ and TS_{P} is small (for SNR values greater than -5 dB), suggesting that the modeling error from the first-order approximations in Propositions 1 and 4 does not substantially degrade performance. Furthermore, the computational complexity of $\mathrm{DPD}_{2\mathrm{CU}}$ and $\mathrm{TS}_{1\mathrm{C}}$ is compared in Table II. The notations n_f and n_τ represent the grid numbers for the frequency shift and time delay used in $\mathrm{TS}_{1\mathrm{C}}$, respectively. N_x, N_y, and N_z denote the grid numbers along the X-, Y-, and Z-axes, respectively, while n_{f_c} and n_{τ_c} correspond to the grid numbers for the frequency shift and time delay of the calibration signal, respectively, and N_c is the number of samples of the calibration signal. As a stationary source is considered in our experiments, we do not search over frequency shift and set $n_f = n_{f_c} = 1$. Other parameters were tuned such that the localization accuracy is not significantly improved with further adjustments, which are set as follows: $n_\tau = 41$, $n_{\tau_c} = 21$, $N_x = N_y = 21$, $N_z = 5$, and $N_c = N = 2000$. Based on 100 randomized simulation runs, the average CPU time for a single run of $\mathrm{TS}_{1\mathrm{C}}$ is 8.22 s, while $\mathrm{DPD}_{2\mathrm{CU}}$ requires an average CPU time of 46.99 s. $\mathrm{DPD}_{2\mathrm{CU}}$ is approximately six times slower than $\mathrm{TS}_{1\mathrm{C}}$, primarily due to the computational overhead introduced by the grid search procedure for calculating the correlation, as well as the additional GS process employed to refine the sensor position estimates.

In Fig. 4, we compare RMSE where the SNR of the calibration signals (denoted by SNRc) ranges from -10 to 15 dB with a step size of 5 dB. When SNRc is low, both $\mathrm{DPD}_{2\mathrm{CU}}$ and $\mathrm{DPD}_{2\mathrm{CNU}}$ outperform $\mathrm{DPD}_{1\mathrm{CU}}$. However, when SNRc$>0$, $\mathrm{DPD}_{1\mathrm{CU}}$ is superior to $\mathrm{DPD}_{2\mathrm{CNU}}$ and is only slightly inferior to the proposed $\mathrm{DPD}_{2\mathrm{CU}}$. The proposed $\mathrm{DPD}_{2\mathrm{CU}}$ always performs the best under each case of SNRc.

In Fig. 5, we fix both SNR and SNRc as -5 dB but the sensor position uncertainty scales linearly with the location uncertainty factor. The performance of $\mathrm{DPD}_{\mathrm{NCNU}}$, $\mathrm{DPD}_{\mathrm{NCU}}$, $\mathrm{DPD}_{1\mathrm{CNU}}$, $\mathrm{DPD}_{1\mathrm{CU}}$, $\mathrm{DPD}_{2\mathrm{CU}}$, and $\mathrm{DPD}_{2\mathrm{CU}}$ is compared, and we observe that $\mathrm{DPD}_{2\mathrm{CU}}$ still performs the best with different location uncertainty factors. Another important finding is that the performance of $\mathrm{DPD}_{\mathrm{NCNU}}$ and $\mathrm{DPD}_{\mathrm{NCU}}$ degrades greatly

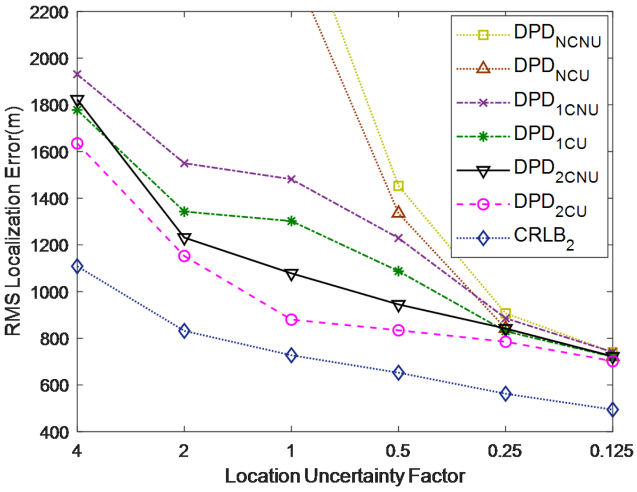

Fig. 5. RMSE of different sensor position uncertainty levels.

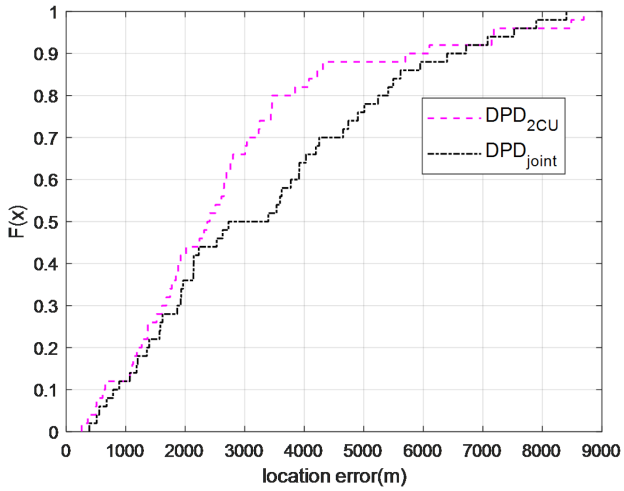

Fig. 6. CDFs of localization errors.

TABLE III
Comparison Between $\mathrm{DPD}_{2\mathrm{CU}}$ and $\mathrm{DPD}_{\mathrm{joint}}$

SNR(dB)	−10	−5	0	5	10	15
$\mathrm{DPD}_{2\mathrm{CU}}$	3391.6	2304.5	1228.2	739.5	478.6	363.2
$\mathrm{DPD}_{\mathrm{joint}}$	3979.9	2553.6	1456.5	779.5	499.4	351.2

when the location uncertainty factor grows large, but the performance of $\mathrm{DPD}_{2\mathrm{CU}}$ degrades only slightly. This again verifies the value of the calibrator and the effectiveness of $\mathrm{DPD}_{2\mathrm{CU}}$.

D. Comparison With Joint Optimization Strategy

This section compares the proposed $\mathrm{DPD}_{2\mathrm{CU}}$ with a joint optimization strategy, denoted by $\mathrm{DPD}_{\mathrm{joint}}$. In the joint optimization strategy, the emitter location and the sensor position are optimized jointly in an alternating manner.

We consider a scenario where SNRc is kept as −15 dB and SNR ranges from −10 to 15 dB with a step size of 5 dB. In addition, the covariance of sensor position uncertainty is set to be equal to the RDOA covariance between sensors 1 and 2 under each SNR. As given in Table III, for high SNR, good initial estimates of sensor positions and emitter location are available, $\mathrm{DPD}_{\mathrm{joint}}$ performs similarly to $\mathrm{DPD}_{2\mathrm{CU}}$, which demonstrate the effectiveness of $\mathrm{DPD}_{\mathrm{joint}}$. However, low SNR (e.g., SNR = −15 dB) leads to poor initial estimates of sensor positions and emitter location, $\mathrm{DPD}_{\mathrm{joint}}$ is inferior to $\mathrm{DPD}_{2\mathrm{CU}}$, which is attributed to the estimates of sensor positions are far from their true values.

Fig. 6 gives a closer look at the performance of $\mathrm{DPD}_{2\mathrm{CU}}$ and $\mathrm{DPD}_{\mathrm{joint}}$ when the SNR is −10 dB by providing the empirical cumulative distribution function (CDF) of all the samples. Both $\mathrm{DPD}_{2\mathrm{CU}}$ and $\mathrm{DPD}_{\mathrm{joint}}$ provide about 50% of samples with location error less than 3000 m. However, $\mathrm{DPD}_{\mathrm{joint}}$ gives more samples with large location error and finally leads to a larger rms localization error.

VI. CONCLUSION

This article considers the problem of emitter localization under conditions where sensors experience positional uncertainties. Using a calibration signal, we have developed a refined GS algorithm as the initial step to effectively address the high-dimensional optimization associated with the sensor position calibration problem. Subsequently, by counting measurement noise as well as the estimation uncertainties in the calibrated sensor positions, we propose a revised DPD formulation. This formulation has demonstrated greater resilience to sensor position uncertainties compared to existing methods. In addition to using calibration signals to reduce sensor position uncertainties, another way to mitigating sensor position uncertainty is utilizing a cooperative synchronization scheme [39], [40] where sensors can communicate with each other. It would be interesting to further investigate the potential of a cooperative synchronization scheme for the DPD paradigm.

APPENDIX A
PROOF OF PROPOSITION 1

For notation simplicity, denote $\frac{\partial \boldsymbol{\eta}\mathbf{Q}(\mathbf{u}^o,\mathbf{s}^o)\mathbf{r}}{\partial \mathbf{s}^o}|_{\mathbf{s}^o=\mathbf{s}}$ as $\frac{\partial \boldsymbol{\eta}\mathbf{Q}\mathbf{r}}{\partial \mathbf{s}^o}$, then according to (6), $\frac{\partial \boldsymbol{\eta}\mathbf{Q}\mathbf{r}}{\partial \mathbf{s}^o}$ can be further expanded as

$$\frac{\partial \boldsymbol{\eta}\mathbf{Q}\mathbf{r}}{\partial \mathbf{s}^o} = \mathrm{blkdiag}\left[\frac{\partial \eta_1 \mathbf{Q}_1\mathbf{r}}{\partial \mathbf{s}_1^o}, \ldots, \frac{\partial \eta_M \mathbf{Q}_M\mathbf{r}}{\partial \mathbf{s}_M^o}\right]$$

where

$$\frac{\partial \eta_i \mathbf{Q}_i\mathbf{r}}{\partial \mathbf{s}_i^o} = \frac{\partial \eta_i \mathbf{Q}_i\mathbf{r}}{\partial \tau_i}\frac{\partial \tau_i}{\mathbf{s}_i^o},\ \frac{\partial \tau_i}{\mathbf{s}_i^o} = \frac{-\left(\mathbf{u}^o - \mathbf{s}_i^o\right)^T}{c\left\|\mathbf{u}^o - \mathbf{s}_i^o\right\|}$$
$$\frac{\partial \eta_i \mathbf{Q}_i\mathbf{r}}{\partial \tau_i} = -j\frac{2\pi}{N\Delta T}\eta_i \mathbf{F}^H \mathbf{D}_{\tau_i}\mathrm{diag}\{\mathbf{n}\}\mathbf{F}\mathbf{r}. \quad (20)$$

Since both $\mathbf{w}$ and $\boldsymbol{\Delta}$ are zero-mean Gaussian noise, we have

$$\mathbb{E}\{\mathbf{v}\} = \frac{\partial \boldsymbol{\eta}\mathbf{Q}(\mathbf{u}^o,\mathbf{s}^o)\mathbf{r}}{\partial \mathbf{s}^o}\mathbb{E}\{\boldsymbol{\Delta}\} + \mathbb{E}\{\mathbf{w}\} = \mathbf{0}.$$

Notice that $\mathbf{w}_i$ and $\mathbf{w}_j$ with $i \neq j$ are statistically independent (the same for $\boldsymbol{\Delta}_i$ and $\boldsymbol{\Delta}_j$), the covariance matrix of $\mathbf{v}$ also has a block diagonal form, given as

$$\boldsymbol{\Lambda}_v = \mathrm{blkdiag}\{\boldsymbol{\Lambda}_{v,1}, \boldsymbol{\Lambda}_{v,2}, \ldots, \boldsymbol{\Lambda}_{v,M}\}$$

where

$$\begin{aligned}\boldsymbol{\Lambda}_{v,i} &= \mathbb{E}\left\{\frac{\partial \eta_i \mathbf{Q}_i \mathbf{r}}{\partial \mathbf{s}_i^o}\mathbb{E}\left\{\boldsymbol{\Delta}_i \boldsymbol{\Delta}_i^T\right\}\left(\frac{\partial \eta_i \mathbf{Q}_i \mathbf{r}}{\partial \mathbf{s}_i^o}\right)^H\right\} + \mathbb{E}\left\{\mathbf{w}_i \mathbf{w}_i^H\right\} \\ &= \sigma_s^2 \mathbb{E}\left\{\frac{\partial \eta_i \mathbf{Q}_i \mathbf{r}}{\partial \mathbf{s}_i^o}\left(\frac{\partial \eta_i \mathbf{Q}_i \mathbf{r}}{\partial \mathbf{s}_i^o}\right)^H\right\} + \sigma_i^2 \mathbf{I}_N.\end{aligned}$$

According to (20), we have

$$\mathbb{E}\left\{\frac{\partial \eta_i \mathbf{Q}_i \mathbf{r}}{\partial \mathbf{s}_i^o}\left(\frac{\partial \eta_i \mathbf{Q}_i \mathbf{r}}{\partial \mathbf{s}_i^o}\right)^H\right\} = \left(\frac{2\pi}{N\Delta T c}\right)^2 \mathbf{H}_i \mathbb{E}\left\{\mathbf{r}\mathbf{r}^H\right\} \mathbf{H}_i^H$$

where $\mathbf{H}_i = \eta_i \mathbf{F}^H \mathbf{D}_{\tau_i} \mathrm{diag}\{\mathbf{n}\}\mathbf{F}$. Using the facts that $\mathbb{E}\{\mathbf{r}\mathbf{r}^H\} = \mathbf{I}_N$ and $\mathbf{F}\mathbf{F}^H = \mathbf{I}_N$, we obtain

$$\begin{aligned}&\mathbb{E}\left\{\frac{\partial \eta_i \mathbf{Q}_i \mathbf{r}}{\partial \mathbf{s}_i^o}\left(\frac{\partial \eta_i \mathbf{Q}_i \mathbf{r}}{\partial \mathbf{s}_i^o}\right)^H\right\} \\ &\quad = \left(\frac{2\pi}{N\Delta T c}\right)^2 |\eta_i|^2 \left(\mathbf{F}^H \mathrm{diag}\left\{\mathbf{n}^2\right\}\mathbf{F}\right). \qquad (21)\end{aligned}$$

Notice that $|\eta_i|^2$ is the signal power at sensor i, which can be estimated as $\hat{P}_i$, and matrix $\mathbf{F}^H \mathrm{diag}\{\mathbf{n}^2\}\mathbf{F}$ is diagonally dominated that can be approximated as $\mathbf{F}^H \mathrm{diag}\{\mathbf{n}^2\}\mathbf{F} \approx \alpha \mathbf{I}_N$, where $\alpha = \mathrm{tr}(\mathbf{F}^H \mathrm{diag}\{\mathbf{n}^2\}\mathbf{F})/N$. Consequentially, we have

$$\boldsymbol{\Lambda}_{v,i} \approx (\alpha \hat{P}_i \left(\frac{2\pi}{N\Delta T c}\right)^2 \sigma_s^2 + \sigma_i^2)\mathbf{I}_N.$$

APPENDIX B
PROOF OF PROPOSITION 2

Denote $\mathbf{Q}_i = \mathbf{Q}_i(\mathbf{u}^o, \mathbf{s})$, Problem (7) can be rewritten as

$$\hat{\mathbf{u}}^o = \arg\min_{\boldsymbol{\eta}, \mathbf{r}, \mathbf{u}^o} \sum_{i=1}^{M} \frac{1}{\varrho_i^2}(\mathbf{z}_i - \eta_i \mathbf{Q}_i \mathbf{r})^H (\mathbf{z}_i - \eta_i \mathbf{Q}_i \mathbf{r}). \qquad (22)$$

Given η_i and $\mathbf{z}_i$, the WLS estimate of $\mathbf{r}$ can be obtained by setting the partial derivative with respect to $\mathbf{r}$ to zero

$$\hat{\mathbf{r}} = \sum_{i=1}^{M} \frac{1}{\varrho_i^2}(\eta_i \mathbf{Q}_i)^H \mathbf{z}_i / \sum_{i=1}^{M} \frac{1}{\varrho_i^2}.$$

Substituting the above expression of $\hat{\mathbf{r}}$ into (22) gives [37]

$$\begin{aligned}\hat{\mathbf{u}}^o &= \arg\min_{\boldsymbol{\eta}, \mathbf{u}^o} \sum_{i=1}^{M} \frac{1}{\varrho_i^2}(\mathbf{z}_i - \eta_i \mathbf{Q}_i \hat{\mathbf{r}})^H (\mathbf{z}_i - \eta_i \mathbf{Q}_i \hat{\mathbf{r}}) \\ &= \arg\max_{\boldsymbol{\eta}, \mathbf{u}^o} \ \boldsymbol{\eta} \cdot \mathbf{R} \cdot \boldsymbol{\eta}^H \qquad (23)\end{aligned}$$

where $\mathbf{R}$ is the correlation matrix with its (i, j)th entity to be

$$R_{ij} = \frac{\mathbf{z}_i^H \mathbf{Q}_i \mathbf{Q}_j^H \mathbf{z}_j}{\varrho_i^2 \varrho_j^2}.$$

As $\boldsymbol{\eta}$ is unknown, the optimal $\boldsymbol{\eta}$ is the scaled eigenvector corresponding to the largest eigenvalue of $\mathbf{R}$. Using this fact, Problem (23) is equivalent to

$$\hat{\mathbf{u}}^o = \arg\max_{\mathbf{u}^o} \ \lambda_{\max}\{\mathbf{R}\}$$

where $\lambda_{\max}\{\mathbf{R}\}$ denotes the maximum eigenvalue of $\mathbf{R}$.

APPENDIX C
PROOF OF PROPOSITION 5

For notation simplicity, denote $\frac{\partial \boldsymbol{\eta}\mathbf{Q}(\mathbf{u}^o, \mathbf{s}^o)\mathbf{r}}{\partial \mathbf{s}^o}|_{\mathbf{s}^o = \bar{\mathbf{s}}^o}$ as $\frac{\partial \boldsymbol{\eta}\mathbf{Q}\mathbf{r}}{\partial \mathbf{s}^o}$, then by invoking the asymptotic normality of the MLE for $\mathbf{s}^o$, we have $\mathbb{E}\{\bar{\mathbf{v}}\} \approx \mathbf{0}$ and

$$\mathrm{Cov}\{\bar{\mathbf{v}}\} = \boldsymbol{\Lambda}_{\bar{v}} = \boldsymbol{\Lambda} + \underbrace{\mathbb{E}\left\{\frac{\partial \boldsymbol{\eta}\mathbf{Q}\mathbf{r}}{\partial \mathbf{s}^o}\Delta\bar{\mathbf{s}}^o \Delta\bar{\mathbf{s}}^{oT}\left(\frac{\partial \boldsymbol{\eta}\mathbf{Q}\mathbf{r}}{\partial \mathbf{s}^o}\right)^H\right\}}_{\boldsymbol{\Lambda}_s}$$

where $\mathbb{E}\left\{\mathbf{w}\mathbf{w}^H\right\} = \boldsymbol{\Lambda}$ is used. As $\mathbf{s}^o$ is estimated from measurement models (1) and (5) under the ML criterion, CRLB can be used to reasonably approximate $\mathbb{E}\{\Delta\bar{\mathbf{s}}^o(\Delta\bar{\mathbf{s}}^o)^T\}$.The FIM of $\mathbf{s}^o$ is given as

$$\begin{aligned}\mathbf{J}_{s^o} &= \left\{\begin{pmatrix}\frac{\partial \boldsymbol{\eta}_c \mathbf{Q}_c \mathbf{r}_c}{\partial \mathbf{s}^o} \\ \frac{\partial \mathbf{s}}{\partial \mathbf{s}^o}\end{pmatrix}^H \begin{pmatrix}\boldsymbol{\Lambda}_c^{-1} & \mathbf{0} \\ \mathbf{0} & \mathbf{Q}_s^{-1}\end{pmatrix}\begin{pmatrix}\frac{\partial \boldsymbol{\eta}_c \mathbf{Q}_c \mathbf{r}_c}{\partial \mathbf{s}^o} \\ \frac{\partial \mathbf{s}}{\partial \mathbf{s}^o}\end{pmatrix}\right\} \\ &= \underbrace{\left(\frac{\partial \boldsymbol{\eta}_c \mathbf{Q}_c \mathbf{r}_c}{\partial \mathbf{s}^o}\right)^H \boldsymbol{\Lambda}_c^{-1}\left(\frac{\partial \boldsymbol{\eta}_c \mathbf{Q}_c \mathbf{r}_c}{\partial \mathbf{s}^o}\right)}_{\mathbf{J}_s} + \mathbf{Q}_s^{-1}.\end{aligned}$$

Concretely, we have $\mathbf{J}_s = \mathrm{blkdiag}\{\mathbf{J}_{s1}, \mathbf{J}_{s2}, \ldots, \mathbf{J}_{sM}\}$, where

$$\mathbf{J}_{si} = \left(\frac{\partial \eta_{ci} \mathbf{Q}_{ci} \mathbf{r}_c}{\partial \mathbf{s}_i^o}\right)^H \left(\frac{\partial \eta_{ci} \mathbf{Q}_{ci} \mathbf{r}_c}{\partial \mathbf{s}_i^o}\right) \sigma_{ci}^{-2}$$

and

$$\begin{aligned}\frac{\partial \eta_{ci} \mathbf{Q}_{ci} \mathbf{r}_c}{\partial \mathbf{s}_i^o} &= \frac{\partial \eta_{ci} \mathbf{Q}_{ci} \mathbf{r}_c}{\partial \tau_{ci}} \frac{\partial \tau_{ci}}{\partial \mathbf{s}_i^o} \\ &= \left(-j\frac{2\pi}{N_c \Delta T} \eta_{ci} \mathbf{F}_c^H \mathbf{D}_{c\tau_i} \mathrm{diag}\{\mathbf{n}_c\} \mathbf{F}_c \mathbf{r}_c\right)\left(\frac{-\left(\mathbf{c}^o - \mathbf{s}_i^o\right)^T}{c\left\|\mathbf{c}^o - \mathbf{s}_i^o\right\|}\right).\end{aligned}$$

Using the facts that $\mathbb{E}\{\mathbf{r}_c \mathbf{r}_c^H\} = \mathbf{I}_{N_c}$ and $\mathbf{F}_c \mathbf{F}_c^H = \mathbf{I}_{N_c}$, we obtain

$$\begin{aligned}&\mathbb{E}\left\{\frac{\partial \eta_{ci} \mathbf{Q}_{ci} \mathbf{r}_c}{\partial \mathbf{s}_i^o}\left(\frac{\partial \eta_{ci} \mathbf{Q}_{ci} \mathbf{r}_c}{\partial \mathbf{s}_i^o}\right)^H\right\} \\ &= \left(\frac{2\pi}{N_c \Delta T c}\right)^2 |\eta_{ci}|^2 \frac{\left(\mathbf{c}^o - \mathbf{s}_i^o\right)}{\left\|\mathbf{c}^o - \mathbf{s}_i^o\right\|} \mathbf{r}_c^H \mathbf{F}_c^H \mathrm{diag}\left\{\mathbf{n}_c{}^2\right\} \mathbf{F}_c \mathbf{r}_c \\ &\quad \times \frac{\left(\mathbf{c}^o - \mathbf{s}_i^o\right)^T}{\left\|\mathbf{c}^o - \mathbf{s}_i^o\right\|} \\ &\approx \alpha_c \left(\frac{2\pi}{N_c \Delta T c}\right)^2 |\eta_{ci}|^2 \frac{\left(\mathbf{c}^o - \mathbf{s}_i^o\right)\left(\mathbf{c}^o - \mathbf{s}_i^o\right)^T}{\left\|\mathbf{c}^o - \mathbf{s}_i^o\right\|^2}\end{aligned}$$

where matrix $\mathbf{F}_c^H \mathrm{diag}\{\mathbf{n}_c^2\}\mathbf{F}_c$ is diagonally dominated and is approximated as $\mathbf{F}_c^H \mathrm{diag}\{\mathbf{n}_c^2\}\mathbf{F}_c \approx \alpha_c \mathbf{I}_{N_c}$ with $\alpha_c = \mathrm{tr}(\mathbf{F}_c^H \mathrm{diag}\{\mathbf{n}_c{}^2\}\mathbf{F}_c)/N_c$. Since $|\eta_{ci}|^2$ is the calibration signal power at sensor i, which can be estimated as $\hat{P}_{ci}$, consequentially, we have

$$\mathbf{J}_{si} = \underbrace{\left(\alpha_c \hat{P}_{ci}\left(\frac{2\pi}{N_c \Delta T c}\right)^2 \sigma_{ci}^{-2}\right)}_{\bar{\alpha}_{ci}} \frac{\left(\mathbf{c}^o - \mathbf{s}_i^o\right)\left(\mathbf{c}^o - \mathbf{s}_i^o\right)^T}{\left\|\mathbf{c}^o - \mathbf{s}_i^o\right\|^2}.$$

Thus, the CRLB for $\mathbf{s}_i^o$ is

$$\begin{aligned}\mathbf{C}_i &= \text{Diag}\left\{\left(\mathbf{J}_{si}+\sigma_s^{-2}\mathbf{I}_3\right)^{-1}\right\}\\ &= \text{Diag}\left\{\sigma_s^2\mathbf{I}_3-\frac{\sigma_s^2\bar{\alpha}_{ci}}{\sigma_s^{-2}+\bar{\alpha}_{ci}}\frac{\left(\mathbf{c}^o-\mathbf{s}_i^o\right)\left(\mathbf{c}^o-\mathbf{s}_i^o\right)^T}{\left\|\mathbf{c}^o-\mathbf{s}_i^o\right\|^2}\right\}\\ &\approx \frac{3\sigma_s^2+2\alpha_{ci}\sigma_s^4}{3+\alpha_{ci}\sigma_s^2}\mathbf{I}_3\end{aligned}$$

where Diag{·} denotes the operation of extracting the diagonal entries from a matrix to form a diagonal matrix, and the second equality is due to the Sherman–Morrison formula. The final approximation is due the fact that the diagonal entries of $(\mathbf{c}^o-\mathbf{s}_i^o)(\mathbf{c}^o-\mathbf{s}_i^o)^T$ are of the same scaling level. Thus, together with block structure of $\frac{\partial\boldsymbol{\eta}\mathbf{Q}\mathbf{r}}{\partial\mathbf{s}^o}$

$$\frac{\partial\boldsymbol{\eta}\mathbf{Q}\mathbf{r}}{\partial\mathbf{s}^o}=\text{blkdiag}\left\{\frac{\partial\eta_1\mathbf{Q}_1\mathbf{r}}{\partial\mathbf{s}_1^o},\ldots,\frac{\partial\eta_M\mathbf{Q}_M\mathbf{r}}{\partial\mathbf{s}_M^o}\right\}$$

we have $\boldsymbol{\Lambda}_s=\text{blkdiag}\{\boldsymbol{\Lambda}_{s1},\boldsymbol{\Lambda}_{s2},\ldots,\boldsymbol{\Lambda}_{sM}\}$, where

$$\boldsymbol{\Lambda}_{si}=\frac{3\sigma_s^2+2\bar{\alpha}_{ci}\sigma_s^4}{3+\bar{\alpha}_{ci}\sigma_s^2}\frac{\partial\eta_i\mathbf{Q}_i\mathbf{r}}{\partial\mathbf{s}_i^o}\left(\frac{\partial\eta_i\mathbf{Q}_i\mathbf{r}}{\partial\mathbf{s}_i^o}\right)^H.$$

Similar to the approximation applied for (21), we have

$$\boldsymbol{\Lambda}_{si}=\left(\frac{3\sigma_s^2+2\bar{\alpha}_{ci}\sigma_s^4}{3+\bar{\alpha}_{ci}\sigma_s^2}\hat{P}_i\left(\frac{2\pi}{N\Delta Tc}\right)^2\right)\mathbf{I}_N.$$

Finally, we have

$$\text{Cov}\{\bar{\mathbf{v}}\}=\text{blkdiag}\left\{\bar{\varrho}_1^2\mathbf{I}_N,\bar{\varrho}_2^2\mathbf{I}_N,\ldots,\bar{\varrho}_M^2\mathbf{I}_N\right\}$$

where

$$\bar{\varrho}_i=\sigma_i^2+\left(\frac{3\sigma_s^2+2\bar{\alpha}_{ci}\sigma_s^4}{3+\bar{\alpha}_{ci}\sigma_s^2}\hat{P}_i\left(\frac{2\pi}{N\Delta Tc}\right)^2\right)\quad\forall i.$$

APPENDIX D
DERIVATION OF CRLB

The CRLB provides a lower bound on the variance of any unbiased estimator, thereby serving as a benchmark for evaluating estimator performance. This section derives the CRLB on the estimation error variance of the emitter position $\mathbf{u}^o$, both without and with the presence of a calibrator.

D1 CRLB Without Calibrator

This section derives the CRLB of $\mathbf{u}^o$ without a calibrator. For notation convenience, the unknown signal $\mathbf{r}$ is expressed in terms of its real and imaginary parts as Re{$\mathbf{r}$} and Im{$\mathbf{r}$}, respectively. Define the composite unknown vector

$$\boldsymbol{\delta}_1=\left[\text{Re}\{\mathbf{r}^T\},\text{Im}\{\mathbf{r}^T\},\boldsymbol{\theta}_1^T\right]^T$$

where $\boldsymbol{\theta}_1=[\boldsymbol{\eta}^T,(\mathbf{s}^o)^T,(\mathbf{u}^o)^T]^T$ and $\boldsymbol{\eta}=[\eta_1,\eta_2,\ldots\eta_M]^T$. According to the position error model (1) and signal model (6), the FIM is the Hessian of the log-likelihood function given as

$$\mathbf{J}_{\delta_1}=2\,\text{Re}\left\{\begin{pmatrix}\frac{\partial\boldsymbol{\eta}\mathbf{Q}\mathbf{r}}{\partial\boldsymbol{\delta}_1}\\ \frac{\partial\mathbf{s}^o}{\partial\boldsymbol{\delta}_1}\end{pmatrix}^H\begin{pmatrix}\boldsymbol{\Lambda}^{-1}&\mathbf{0}\\ \mathbf{0}&\mathbf{Q}_s^{-1}\end{pmatrix}\begin{pmatrix}\frac{\partial\boldsymbol{\eta}\mathbf{Q}\mathbf{r}}{\partial\boldsymbol{\delta}_1}\\ \frac{\partial\mathbf{s}^o}{\partial\boldsymbol{\delta}_1}\end{pmatrix}\right\}$$

Following the basic linear algebra derivation and using the partitioned matrix inversion formula (with details provided in Appendix D3), the FIM of $\boldsymbol{\theta}_1$ can be expressed as

$$\mathbf{J}_{\boldsymbol{\theta}_1}=2\mathbf{C}_1-2\,\text{Re}\left\{\mathbf{B}_1\mathbf{A}_1^{-1}\mathbf{B}_1^H\right\}$$

where

$$\mathbf{A}_1=(\boldsymbol{\eta}\mathbf{Q})^H\boldsymbol{\Lambda}^{-1}(\boldsymbol{\eta}\mathbf{Q}),\ \mathbf{B}_1=\left(\frac{\partial\boldsymbol{\eta}\mathbf{Q}\mathbf{r}}{\partial\boldsymbol{\theta}_1}\right)^H\boldsymbol{\Lambda}^{-1}(\boldsymbol{\eta}\mathbf{Q})$$

$$\mathbf{C}_1=\left(\frac{\partial\boldsymbol{\eta}\mathbf{Q}\mathbf{r}}{\partial\boldsymbol{\theta}_1}\right)^H\boldsymbol{\Lambda}^{-1}\left(\frac{\partial\boldsymbol{\eta}\mathbf{Q}\mathbf{r}}{\partial\boldsymbol{\theta}_1}\right)+\left(\frac{\partial\mathbf{s}^o}{\partial\boldsymbol{\theta}_1}\right)^H\mathbf{Q}_s^{-1}\left(\frac{\partial\mathbf{s}^o}{\partial\boldsymbol{\theta}_1}\right).$$

Note that the lower right 2×2 submatrix of $\mathbf{J}_{\boldsymbol{\theta}_1}^{-1}$ corresponds to the CRLB on the estimation error variance of $\mathbf{u}^o$, denoted as crlb_1. The square root of the trace of crlb_1 gives the CRLB on the localization error, denoted as $\text{CRLB}_1=\sqrt{\text{trace}(\text{crlb}_1)}$.

D2 CRLB With Calibrator

To derive the CRLB of $\mathbf{u}^o$ with a calibrator, the calibration signal $\mathbf{r}_c$ is further expressed in terms of its real and imaginary parts as Re{$\mathbf{r}_c$} and Im{$\mathbf{r}_c$}, respectively. Define the composite unknown vector

$$\boldsymbol{\delta}_2=\left[\text{Re}\{\mathbf{r}^T\},\text{Im}\{\mathbf{r}^T\},\text{Re}\{\mathbf{r}_c^T\},\text{Im}\{\mathbf{r}_c^T\},\boldsymbol{\theta}_2^T\right]^T$$

where

$$\boldsymbol{\theta}_2=\left[\boldsymbol{\eta}^T,\boldsymbol{\eta}_c^T,\left(\mathbf{s}^o\right)^T,\left(\mathbf{u}^o\right)^T\right]^T,\ \boldsymbol{\eta}_c=[\eta_{c1},\eta_{c2},\ldots\eta_{cM}]^T.$$

Similarly, based on the position error model (1) and signal models (5) and (6), the FIM can be expressed as

$$\mathbf{J}_{\delta_2}=2\,\text{Re}\left\{\begin{pmatrix}\frac{\partial\boldsymbol{\eta}\mathbf{Q}\mathbf{r}}{\partial\boldsymbol{\delta}_2}\\ \frac{\partial\boldsymbol{\eta}_c\mathbf{Q}_c\mathbf{r}_c}{\partial\boldsymbol{\delta}_2}\\ \frac{\partial\mathbf{s}^o}{\partial\boldsymbol{\delta}_2}\end{pmatrix}^H\begin{pmatrix}\boldsymbol{\Lambda}^{-1}&\mathbf{0}&\mathbf{0}\\ \mathbf{0}&\boldsymbol{\Lambda}_c^{-1}&\mathbf{0}\\ \mathbf{0}&\mathbf{0}&\mathbf{Q}_s^{-1}\end{pmatrix}\begin{pmatrix}\frac{\partial\boldsymbol{\eta}\mathbf{Q}\mathbf{r}}{\partial\boldsymbol{\delta}_2}\\ \frac{\partial\boldsymbol{\eta}_c\mathbf{Q}_c\mathbf{r}_c}{\partial\boldsymbol{\delta}_2}\\ \frac{\partial\mathbf{s}^o}{\partial\boldsymbol{\delta}_2}\end{pmatrix}\right\}.$$

Using the matrix inversion formula (with details provided in Appendix D4), the FIM of $\boldsymbol{\theta}_2$ is

$$\mathbf{J}_{\boldsymbol{\theta}_2}=2\mathbf{C}_2-2\,\text{Re}\left\{\mathbf{B}_2\mathbf{A}_2^{-1}\mathbf{B}_2^H\right\}$$

where

$$\mathbf{A}_2=\begin{bmatrix}\left(\frac{\partial\boldsymbol{\eta}\mathbf{Q}\mathbf{r}}{\partial\mathbf{r}}\right)^H\boldsymbol{\Lambda}^{-1}\left(\frac{\partial\boldsymbol{\eta}\mathbf{Q}\mathbf{r}}{\partial\mathbf{r}}\right)&\mathbf{0}_{N\times N}\\ \mathbf{0}_{N\times N}&\left(\frac{\partial\boldsymbol{\eta}_c\mathbf{Q}_c\mathbf{r}_c}{\partial\mathbf{r}_c}\right)^H\boldsymbol{\Lambda}_c^{-1}\left(\frac{\partial\boldsymbol{\eta}_c\mathbf{Q}_c\mathbf{r}_c}{\partial\mathbf{r}_c}\right)\end{bmatrix}$$

$$\mathbf{B}_2=\begin{bmatrix}\left(\frac{\partial\boldsymbol{\eta}\mathbf{Q}\mathbf{r}}{\partial\boldsymbol{\theta}_2}\right)^H\boldsymbol{\Lambda}^{-1}\left(\frac{\partial\boldsymbol{\eta}\mathbf{Q}\mathbf{r}}{\partial\mathbf{r}}\right)&\left(\frac{\partial\boldsymbol{\eta}_c\mathbf{Q}_c\mathbf{r}_c}{\partial\boldsymbol{\theta}_2}\right)^H\boldsymbol{\Lambda}_c^{-1}\left(\frac{\partial\boldsymbol{\eta}_c\mathbf{Q}_c\mathbf{r}_c}{\partial\mathbf{r}_c}\right)\end{bmatrix}$$

$$\mathbf{C}_2=\left(\frac{\partial\boldsymbol{\eta}\mathbf{Q}\mathbf{r}}{\partial\boldsymbol{\theta}_2}\right)^H\boldsymbol{\Lambda}^{-1}\left(\frac{\partial\boldsymbol{\eta}\mathbf{Q}\mathbf{r}}{\partial\boldsymbol{\theta}_2}\right)+\left(\frac{\partial\mathbf{s}^o}{\partial\boldsymbol{\theta}_2}\right)^H\mathbf{Q}_s^{-1}\left(\frac{\partial\mathbf{s}^o}{\partial\boldsymbol{\theta}_2}\right)+\left(\frac{\partial\boldsymbol{\eta}_c\mathbf{Q}_c\mathbf{r}_c}{\partial\boldsymbol{\theta}_2}\right)^H\boldsymbol{\Lambda}_c^{-1}\left(\frac{\partial\boldsymbol{\eta}_c\mathbf{Q}_c\mathbf{r}_c}{\partial\boldsymbol{\theta}_2}\right).$$

The lower right 2×2 submatrix of $\mathbf{J}_{\boldsymbol{\theta}_2}^{-1}$ is the CRLB of $\mathbf{u}^o$, denoted as crlb_2, and the CRLB on the localization error is $\text{CRLB}_2=\sqrt{\text{trace}(\text{crlb}_2)}$.

D3 Derivation of CRLB Without Calibrator

Recall notation in Appendix D1, we have

$$\frac{\partial \boldsymbol{\eta}\mathbf{Q}\mathbf{r}}{\partial \boldsymbol{\delta}_1} = \left[\frac{\partial \boldsymbol{\eta}\mathbf{Q}\mathbf{r}}{\partial \operatorname{Re}\{\mathbf{r}\}}, \frac{\partial \boldsymbol{\eta}\mathbf{Q}\mathbf{r}}{\partial \operatorname{Im}\{\mathbf{r}\}}, \frac{\partial \boldsymbol{\eta}\mathbf{Q}\mathbf{r}}{\partial \boldsymbol{\theta}_1}\right]$$

$$\frac{\partial \boldsymbol{\eta}\mathbf{Q}\mathbf{r}}{\partial \operatorname{Re}\{\mathbf{r}\}} = \boldsymbol{\eta}\mathbf{Q}, \quad \frac{\partial \boldsymbol{\eta}\mathbf{Q}\mathbf{r}}{\partial \operatorname{Im}\{\mathbf{r}\}} = j\boldsymbol{\eta}\mathbf{Q}$$

$$\frac{\partial \boldsymbol{\eta}\mathbf{Q}\mathbf{r}}{\partial \boldsymbol{\theta}_1} = \left[\left(\frac{\partial \eta_1 \mathbf{Q}_1 \mathbf{r}}{\partial \boldsymbol{\theta}_1}\right)^H, \ldots, \left(\frac{\partial \eta_M \mathbf{Q}_M \mathbf{r}}{\partial \boldsymbol{\theta}_1}\right)^H\right]^H$$

where

$$\frac{\partial \eta_i \mathbf{Q}_i \mathbf{r}}{\partial \boldsymbol{\theta}_1} = \left[\frac{\partial \eta_i \mathbf{Q}_i \mathbf{r}}{\partial \boldsymbol{\eta}}, \frac{\partial \eta_i \mathbf{Q}_i \mathbf{r}}{\partial \mathbf{s}^o}, \frac{\partial \eta_i \mathbf{Q}_i \mathbf{r}}{\partial \mathbf{u}^o}\right]$$

$$\frac{\partial \eta_i \mathbf{Q}_i \mathbf{r}}{\partial \boldsymbol{\eta}} = \left[\frac{\partial \eta_i \mathbf{Q}_i \mathbf{r}}{\partial \eta_1}, \ldots, \frac{\partial \eta_i \mathbf{Q}_i \mathbf{r}}{\partial \eta_M}\right]$$

$$\frac{\partial \eta_i \mathbf{Q}_i \mathbf{r}}{\partial \mathbf{s}^o} = \left[\frac{\partial \eta_i \mathbf{Q}_i \mathbf{r}}{\partial \mathbf{s}_1^o}, \ldots, \frac{\partial \eta_i \mathbf{Q}_i \mathbf{r}}{\partial \mathbf{s}_M^o}\right].$$

Specifically, according to (4), we have

$$\frac{\partial \eta_i \mathbf{Q}_i \mathbf{r}}{\partial \eta_n} = \begin{cases} \mathbf{Q}_i \mathbf{r}, & i = n \\ 0, & i \neq n \end{cases}$$

$$\frac{\partial \eta_i \mathbf{Q}_i \mathbf{r}}{\partial \mathbf{s}_n^o} = \begin{cases} \frac{\partial \eta_i \mathbf{Q}_i \mathbf{r}}{\partial \tau_i} \frac{\partial \tau_i}{\partial \mathbf{s}_n^o}, & i = n \\ 0, & i \neq n \end{cases}$$

$$\frac{\partial \eta_i \mathbf{Q}_i \mathbf{r}}{\partial \mathbf{u}^o} = \frac{\partial \eta_i \mathbf{Q}_i \mathbf{r}}{\partial \tau_i} \frac{\partial \tau_i}{\partial \mathbf{u}^o}$$

where

$$\frac{\partial \eta_i \boldsymbol{\Phi}_i \mathbf{Q}_i \mathbf{s}}{\partial \tau_i} = -j\frac{2\pi}{N\Delta} \eta_i \mathbf{F}^H \mathbf{D}_{\tau_i} \operatorname{diag}\{\tilde{\mathbf{n}}\} \mathbf{F}\mathbf{r}$$

$$\frac{\partial \tau_i}{\partial \mathbf{u}^o} = \frac{\left(\mathbf{u}^o - \mathbf{s}_i^o\right)^T}{c\left\|\mathbf{u}^o - \mathbf{s}_i^o\right\|} = -\frac{\partial \tau_i}{\partial \mathbf{s}_i^o}.$$

By definition of $\boldsymbol{\delta}_1$, we have

$$\frac{\partial \mathbf{s}^o}{\partial \boldsymbol{\delta}_1} = \left[\mathbf{0}, \mathbf{0}, \frac{\partial \mathbf{s}^o}{\partial \boldsymbol{\theta}_1}\right], \quad \frac{\partial \mathbf{s}^o}{\partial \boldsymbol{\theta}_1} = \left[\mathbf{0}, \mathbf{I}_{3M}, \mathbf{0}\right].$$

Thus, we have

$$\mathbf{J}_{\boldsymbol{\delta}_1} = 2\begin{bmatrix} \mathbf{A}_1 & \mathbf{0} & \operatorname{Re}\{\mathbf{B}_1^H\} \\ \mathbf{0} & \mathbf{A}_1 & \operatorname{Im}\{\mathbf{B}_1^H\} \\ \operatorname{Re}\{\mathbf{B}_1\} & -\operatorname{Im}\{\mathbf{B}_1\} & \mathbf{C}_1 \end{bmatrix}$$

where

$$\mathbf{A}_1 = (\boldsymbol{\eta}\mathbf{Q})^H \boldsymbol{\Lambda}^{-1} (\boldsymbol{\eta}\mathbf{Q}), \ \mathbf{B}_1 = \left(\frac{\partial \boldsymbol{\eta}\mathbf{Q}\mathbf{r}}{\partial \boldsymbol{\theta}_1}\right)^H \boldsymbol{\Lambda}^{-1} (\boldsymbol{\eta}\mathbf{Q})$$

$$\mathbf{C}_1 = \left(\frac{\partial \boldsymbol{\eta}\mathbf{Q}\mathbf{r}}{\partial \boldsymbol{\theta}_1}\right)^H \boldsymbol{\Lambda}^{-1} \left(\frac{\partial \boldsymbol{\eta}\mathbf{Q}\mathbf{r}}{\partial \boldsymbol{\theta}_1}\right) + \left(\frac{\partial \mathbf{s}^o}{\partial \boldsymbol{\theta}_1}\right)^H \mathbf{Q}_s^{-1} \left(\frac{\partial \mathbf{s}^o}{\partial \boldsymbol{\theta}_1}\right).$$

Hence, by the block matrix inversion formula, we have

$$\mathbf{J}_{\boldsymbol{\theta}_1} = 2\mathbf{C}_1 - 2\operatorname{Re}\left\{\mathbf{B}_1 \mathbf{A}_1^{-1} \mathbf{B}_1^H\right\}.$$

D4 Derivation of CRLB With Calibrator

Recall notation in Appendix D2, we have

$$\frac{\partial \boldsymbol{\eta}\mathbf{Q}\mathbf{r}}{\partial \boldsymbol{\delta}_2} = \left[\frac{\partial \boldsymbol{\eta}\mathbf{Q}\mathbf{r}}{\partial \mathbf{r}}, \frac{\partial \boldsymbol{\eta}\mathbf{Q}\mathbf{r}}{\partial \mathbf{r}_c}, \frac{\partial \boldsymbol{\eta}\mathbf{Q}\mathbf{r}}{\partial \boldsymbol{\theta}_2}\right]$$

$$\frac{\partial \boldsymbol{\eta}\mathbf{Q}\mathbf{r}}{\partial \mathbf{r}} = \left[\frac{\partial \boldsymbol{\eta}\mathbf{Q}\mathbf{r}}{\partial \operatorname{Re}\{\mathbf{r}\}}, \frac{\partial \boldsymbol{\eta}\mathbf{Q}\mathbf{r}}{\partial \operatorname{Im}\{\mathbf{r}\}}\right]$$

$$\frac{\partial \boldsymbol{\eta}\mathbf{Q}\mathbf{r}}{\partial \mathbf{r}_c} = \left[\frac{\partial \boldsymbol{\eta}\mathbf{Q}\mathbf{r}}{\partial \operatorname{Re}\{\mathbf{r}_c\}}, \frac{\partial \boldsymbol{\eta}\mathbf{Q}\mathbf{r}}{\partial \operatorname{Im}\{\mathbf{r}_c\}}\right], \quad \frac{\partial \boldsymbol{\eta}\mathbf{Q}\mathbf{r}}{\partial \operatorname{Re}\{\mathbf{r}\}} = \boldsymbol{\eta}\mathbf{Q}$$

$$\frac{\partial \boldsymbol{\eta}\mathbf{Q}\mathbf{r}}{\partial \operatorname{Im}\{\mathbf{r}\}} = j\boldsymbol{\eta}\mathbf{Q}, \quad \frac{\partial \boldsymbol{\eta}\mathbf{Q}\mathbf{r}}{\partial \operatorname{Re}\{\mathbf{r}_c\}} = \frac{\partial \boldsymbol{\eta}\mathbf{Q}\mathbf{r}}{\partial \operatorname{Im}\{\mathbf{r}_c\}} = \mathbf{0}$$

$$\frac{\partial \boldsymbol{\eta}\mathbf{Q}\mathbf{r}}{\partial \boldsymbol{\theta}_2} = \left[\left(\frac{\partial \eta_1 \mathbf{Q}_1 \mathbf{r}}{\partial \boldsymbol{\theta}_2}\right)^H, \ldots, \left(\frac{\partial \eta_M \mathbf{Q}_M \mathbf{r}}{\partial \boldsymbol{\theta}_2}\right)^H\right]^H$$

where

$$\frac{\partial \eta_i \mathbf{Q}_i \mathbf{r}}{\partial \boldsymbol{\theta}_2} = \left[\frac{\partial \eta_i \mathbf{Q}_i \mathbf{r}}{\partial \boldsymbol{\eta}}, \frac{\partial \eta_i \mathbf{Q}_i \mathbf{r}}{\partial \boldsymbol{\eta}_c}, \frac{\partial \eta_i \mathbf{Q}_i \mathbf{r}}{\partial \mathbf{s}^o}, \frac{\partial \eta_i \mathbf{Q}_i \mathbf{r}}{\partial \mathbf{u}^o}\right]$$

$$\frac{\partial \eta_i \mathbf{Q}_i \mathbf{r}}{\partial \boldsymbol{\eta}_c} = \mathbf{0}_{N \times M}.$$

And similarly, for the calibration signal part, we have

$$\frac{\partial \boldsymbol{\eta}_c \mathbf{Q}_c \mathbf{r}_c}{\partial \boldsymbol{\delta}_2} = \left[\frac{\partial \boldsymbol{\eta}_c \mathbf{Q}_c \mathbf{r}_c}{\partial \operatorname{Re}\{\mathbf{r}\}}, \frac{\partial \boldsymbol{\eta}_c \mathbf{Q}_c \mathbf{r}_c}{\partial \operatorname{Im}\{\mathbf{r}\}}, \frac{\partial \boldsymbol{\eta}_c \mathbf{Q}_c \mathbf{r}_c}{\partial \operatorname{Re}\{\mathbf{r}_c\}}, \frac{\partial \boldsymbol{\eta}_c \mathbf{Q}_c \mathbf{r}_c}{\partial \operatorname{Im}\{\mathbf{r}_c\}}, \frac{\partial \boldsymbol{\eta}_c \mathbf{Q}_c \mathbf{r}_c}{\partial \boldsymbol{\theta}_2}\right]$$

$$\frac{\partial \boldsymbol{\eta}_c \mathbf{Q}_c \mathbf{r}_c}{\partial \operatorname{Re}\{\mathbf{r}\}} = \frac{\partial \boldsymbol{\eta}_c \mathbf{Q}_c \mathbf{r}_c}{\partial \operatorname{Im}\{\mathbf{r}\}} = \mathbf{0}_{MN \times N}$$

$$\frac{\partial \boldsymbol{\eta}_c \mathbf{Q}_c \mathbf{r}_c}{\partial \operatorname{Re}\{\mathbf{r}_c\}} = \boldsymbol{\eta}_c \mathbf{Q}_c, \quad \frac{\partial \boldsymbol{\eta}_c \mathbf{Q}_c \mathbf{r}_c}{\partial \operatorname{Im}\{\mathbf{r}_c\}} = j\boldsymbol{\eta}_c \mathbf{Q}_c$$

$$\frac{\partial \boldsymbol{\eta}_c \mathbf{Q}_c \mathbf{r}_c}{\partial \boldsymbol{\theta}_2} = \left[\left(\frac{\partial \eta_{c1} \mathbf{Q}_{c1} \mathbf{r}_c}{\partial \boldsymbol{\theta}_2}\right)^H, \ldots, \left(\frac{\partial \eta_{cM} \mathbf{Q}_{cM} \mathbf{r}_c}{\partial \boldsymbol{\theta}_2}\right)^H\right]^H$$

where

$$\frac{\partial \eta_{ci} \mathbf{Q}_{ci} \mathbf{r}_{ci}}{\partial \boldsymbol{\theta}_2} = \left[\frac{\partial \eta_{ci} \mathbf{Q}_{ci} \mathbf{r}_c}{\partial \boldsymbol{\eta}}, \frac{\partial \eta_{ci} \mathbf{Q}_{ci} \mathbf{r}_c}{\partial \boldsymbol{\eta}_c}, \frac{\partial \eta_{ci} \mathbf{Q}_{ci} \mathbf{r}_c}{\partial \mathbf{s}^o}, \frac{\partial \eta_{ci} \mathbf{Q}_{ci} \mathbf{r}_c}{\partial \mathbf{u}^o}\right]$$

$$\frac{\partial \eta_{ci} \mathbf{Q}_{ci} \mathbf{r}_c}{\partial \boldsymbol{\eta}} = \left[\frac{\partial \eta_{ci} \mathbf{Q}_{ci} \mathbf{r}_c}{\partial \alpha_1}, \ldots, \frac{\partial \eta_{ci} \mathbf{Q}_{ci} \mathbf{r}_c}{\partial \alpha_M}\right]$$

$$\frac{\partial \eta_{ci} \mathbf{Q}_{ci} \mathbf{r}_c}{\partial \boldsymbol{\eta}_c} = \left[\frac{\partial \eta_{ci} \mathbf{Q}_{ci} \mathbf{r}_c}{\partial \alpha_{c1}}, \ldots, \frac{\partial \eta_{ci} \mathbf{Q}_{ci} \mathbf{r}_c}{\partial \alpha_{cM}}\right]$$

$$\frac{\partial \eta_{ci} \mathbf{Q}_{ci} \mathbf{r}_c}{\partial \mathbf{s}^o} = \left[\frac{\partial \eta_{ci} \mathbf{Q}_{ci} \mathbf{r}_c}{\partial \mathbf{s}_1^o}, \ldots, \frac{\partial \eta_{ci} \mathbf{Q}_{ci} \mathbf{r}_c}{\partial \mathbf{s}_M^o}\right].$$

Specifically, according to (3), we have

$$\frac{\partial \eta_{ci} \mathbf{Q}_{ci} \mathbf{r}_c}{\partial \eta_n} = 0$$

$$\frac{\partial \eta_{ci} \mathbf{Q}_{ci} \mathbf{r}_c}{\partial \eta_{cn}} = \begin{cases} \mathbf{Q}_{ci} \mathbf{r}_c, & i = n \\ 0, & i \neq n \end{cases}$$

$$\frac{\partial \eta_{ci} \mathbf{Q}_{ci} \mathbf{r}_c}{\partial \mathbf{s}_n^o} = \begin{cases} \frac{\partial \eta_{ci} \mathbf{Q}_{ci} \mathbf{r}_c}{\partial \tau_{ci}} \frac{\partial \tau_{ci}}{\partial \mathbf{s}_n^o}, & i = n \\ 0, & i \neq n \end{cases}$$

and

$$\frac{\partial \eta_{ci}\mathbf{Q}_{ci}\mathbf{r}_{ci}}{\partial \mathbf{u}^o} = 0.$$

Further, we have

$$\frac{\partial \eta_{ci}\mathbf{Q}_{ci}\mathbf{r}_c}{\partial \tau_i} = -j\frac{2\pi}{N\Delta}\eta_{ci}\mathbf{F}_c^H\mathbf{D}_{\tau_{ci}}\mathrm{diag}\{\tilde{\mathbf{n}}\}\mathbf{F}_c\mathbf{r}_c$$

$$\frac{\partial \tau_{ci}}{\partial \mathbf{s}_i^o} = -\frac{\left(\mathbf{c}^o - \mathbf{s}_i^o\right)^T}{c\left\|\mathbf{c}^o - \mathbf{s}_i^o\right\|}.$$

By definition of $\boldsymbol{\delta}_2$, we have

$$\frac{\partial \mathbf{s}^o}{\partial \boldsymbol{\delta}_2} = \left[\mathbf{0}_{3M\times N}, \mathbf{0}_{3M\times N}, \mathbf{0}_{3M\times N}, \mathbf{0}_{3M\times N}, \frac{\partial \mathbf{s}^o}{\partial \boldsymbol{\theta}_2}\right]$$

where

$$\frac{\partial \mathbf{s}^o}{\partial \boldsymbol{\theta}_2} = \left[\mathbf{0}_{3M\times M}, \mathbf{0}_{3M\times M}, \mathbf{I}_{3M}, \mathbf{0}_{3M\times 3}\right].$$

Thus, we have

$$\mathbf{J}_{\delta_2} = 2\,\mathrm{Re}\begin{bmatrix}\mathbf{A}_2 & \mathbf{B}_2^H\\ \mathbf{B}_2 & \mathbf{C}_2\end{bmatrix}$$

where

$$\mathbf{A}_2 = \begin{bmatrix}\left(\frac{\partial \boldsymbol{\eta}\mathbf{Q}\mathbf{r}}{\partial \mathbf{r}}\right)^H \boldsymbol{\Lambda}^{-1}\left(\frac{\partial \boldsymbol{\eta}\mathbf{Q}\mathbf{r}}{\partial \mathbf{r}}\right) & \mathbf{0}_{N\times N}\\ \mathbf{0}_{N\times N} & \left(\frac{\partial \boldsymbol{\eta}_c\mathbf{Q}_c\mathbf{r}_c}{\partial \mathbf{r}_c}\right)^H \boldsymbol{\Lambda}_c^{-1}\left(\frac{\partial \boldsymbol{\eta}_c\mathbf{Q}_c\mathbf{r}_c}{\partial \mathbf{r}_c}\right)\end{bmatrix}$$

$$\mathbf{B}_2 = \begin{bmatrix}\left(\frac{\partial \boldsymbol{\eta}\mathbf{Q}\mathbf{r}}{\partial \boldsymbol{\theta}_2}\right)^H \boldsymbol{\Lambda}^{-1}\left(\frac{\partial \boldsymbol{\eta}\mathbf{Q}\mathbf{r}}{\partial \mathbf{r}}\right) & \left(\frac{\partial \boldsymbol{\eta}_c\mathbf{Q}_c\mathbf{r}_c}{\partial \boldsymbol{\theta}_2}\right)^H \boldsymbol{\Lambda}_c^{-1}\left(\frac{\partial \boldsymbol{\eta}_c\mathbf{Q}_c\mathbf{r}_c}{\partial \mathbf{r}_c}\right)\end{bmatrix}$$

$$\mathbf{C}_2 = \left(\frac{\partial \boldsymbol{\eta}\mathbf{Q}\mathbf{r}}{\partial \boldsymbol{\theta}_2}\right)^H \boldsymbol{\Lambda}^{-1}\left(\frac{\partial \boldsymbol{\eta}\mathbf{Q}\mathbf{r}}{\partial \boldsymbol{\theta}_2}\right) + \left(\frac{\partial \mathbf{s}^o}{\partial \boldsymbol{\theta}_2}\right)^H \mathbf{Q}_s^{-1}\left(\frac{\partial \mathbf{s}^o}{\partial \boldsymbol{\theta}_2}\right) + \left(\frac{\partial \boldsymbol{\eta}_c\mathbf{Q}_c\mathbf{r}_c}{\partial \boldsymbol{\theta}_2}\right)^H \boldsymbol{\Lambda}_c^{-1}\left(\frac{\partial \boldsymbol{\eta}_c\mathbf{Q}_c\mathbf{r}_c}{\partial \boldsymbol{\theta}_2}\right).$$

Hence, by the block matrix inversion formula, we have $\boldsymbol{\theta}_2$ is

$$\mathbf{J}_{\boldsymbol{\theta}_2} = 2\mathbf{C}_2 - 2\,\mathrm{Re}\left\{\mathbf{B}_2\mathbf{A}_2^{-1}\mathbf{B}_2^H\right\}.$$

REFERENCES

[1] K. C. Ho and W. Xu, "An accurate algebraic solution for moving source location using TDOA and FDOA measurements," *IEEE Trans. Signal Process.*, vol. 52, no. 9, pp. 2453–2463, Sep. 2004.

[2] Y. T. Chan and K. C. Ho, "Simple and efficient estimator for hyperbolic location," *IEEE Trans. Signal Process.*, vol. 42, no. 8, pp. 1905–1915, Aug. 1994.

[3] K. C. Ho and L. Yang, "On the use of a calibration emitter for source localization in the presence of sensor position uncertainty," *IEEE Trans. Signal Process.*, vol. 56, no. 1, pp. 5758–5772, Dec. 2008.

[4] X. Qu, L. Xie, and W. Tan, "Iterative constrained weighted least squares source localization using TDOA and FDOA measurements," *IEEE Trans. Signal Process.*, vol. 65, no. 15, pp. 3900–4003, Aug. 2017.

[5] T. Tirer and A. J. Weiss, "Performance analysis of a high-resolution direct position determination method," *IEEE Trans. Signal Process.*, vol. 65, no. 3, pp. 544–554, Feb. 2017.

[6] A. Amar and A. J. Weiss, "Localization of narrowband radio emitters based on Doppler frequency shifts," *IEEE Trans. Signal Process.*, vol. 56, no. 11, pp. 5500–5508, Nov. 2008.

[7] O. Jean and A. J. Weiss, "Geolocation by direction of arrival using arrays with unknown orientation," *IEEE Trans. Signal Process.*, vol. 62, no. 12, pp. 3135–3142, Jun. 2014.

[8] T.-K. Le and O. Nobutaka, "Closed-form and near closed-form solutions for TOA-based joint source and sensor localization," *IEEE Trans. Signal Process.*, vol. 64, no. 18, pp. 4751–4766, Sep. 2016.

[9] K. W. Cheung, H. C. So, W. -K. Ma, and Y. T. Chan, "Least squares algorithms for time-of-arrival based mobile location," *IEEE Trans. Signal Process.*, vol. 52, no. 4, pp. 1121–1128, Apr. 2004.

[10] Y. T. Chan and K. C. Ho, "A simple and efficient estimator for hyperbolic location," *IEEE Trans. Signal Process.*, vol. 42, no. 8, pp. 1905–1915, Aug. 1994.

[11] D. Musicki, R. Kaune, and W. Koch, "Mobile emitter geolocation and tracking using TDOA and FDOA measurements," *IEEE Trans. Signal Process.*, vol. 58, no. 3, pp. 1863–1874, Mar. 2010.

[12] K. C. Pine, S. Pine, and M. Cheney, "The geometry of far-field passive source localization with TDOA and FDOA," *IEEE Trans. Aerosp. Electron. Syst.*, vol. 57, no. 6, pp. 3782–3790, Dec. 2021.

[13] H. Yu, G. Huang, J. Gao, and B. Liu, "An efficient constrained weighted least squares algorithm for moving source location using TDOA and FDOA measurements," *IEEE Trans. Wireless Commun.*, vol. 11, no. 1, pp. 44–47, Jan. 2012.

[14] D. Jin, H. Yin, C. Fritsche, F. Gustafsson, and A. M. Zoubir, "Bayesian cooperative localization using received signal strength with unknown path loss exponent: Message passing approaches," *IEEE Trans. Signal Process.*, vol. 68, pp. 1120–1135, 2020.

[15] M. Lohrasbipeydeh, T. A. Guliver, and H. Amindavar, "Blind received signal strength difference based source localization with system parameter errors," *IEEE Trans. Signal Process.*, vol. 62, no. 17, pp. 4516–4531, Sep. 2014.

[16] H. Yu, G. Huang, J. Gao, and B. Liu, "An efficient constrained least squares algorithm for moving source location using TDOA and FDOA measurements," *IEEE Trans. Wireless Commun.*, vol. 11, no. 1, pp. 44–47, Jan. 2012.

[17] K. C. Ho and Y. T. Chan, "Geolocation of a known altitude object from TDOA and FDOA measurements," *IEEE Trans. Aerosp. Electron. Syst.*, vol. 33, no. 3, pp. 770–783, Jul. 1997.

[18] A. J. Weiss, "Direct geolocation for wideband emitters based on delay and Doppler," *IEEE Trans. Signal Process.*, vol. 59, no. 6, pp. 2513–2521, Jun. 2011.

[19] J. Li, L. Yang, F. Guo, and W. Jiang, "Coherent summation of multiple short-time signals for direct positioning of a wideband source based on delay and Doppler," *Digit. Signal Process.*, vol. 48, pp. 58–70, 2016.

[20] F. Ma, F. Guo, and L. Yang, "Direct position determination of moving sources based on delay and Doppler," *IEEE Sensors J.*, vol. 20, no. 14, pp. 7859–7869, Jul. 2020.

[21] A. Yeredor, "On passive TDOA and FDOA localization using two sensors with no time or frequency synchronization," in *Proc. IEEE Int. Conf. Acoust., Speech Signal Process.*, 2013, pp. 4066–4070.

[22] L. Youming and M. H. Er, "Theoretical analyses of gain and phase error calibration with optimal implementation for linear equispaced array," *IEEE Trans. Signal Process.*, vol. 54, no. 2, pp. 712–723, Feb. 2006.

[23] K. C. Ho, X. Lu, and L. Kovavisaruch, "Source localization using TDOA and FDOA measurements in the presence of receiver location errors: Analysis and solution," *IEEE Trans. Signal Process.*, vol. 55, no. 2, pp. 684–696, Feb. 2007.

[24] A. Amar and A. J. Weiss, "Direct position determination in the presence of model errors - known waveforms," *Digit. Signal Process.*, vol. 16, pp. 52–83, 2016.

[25] M. Sun and K. C. Ho, "An asymptotically efficient estimator for TDOA and FDOA positioning of multiple disjoint sources in the presence of sensor location uncertainties," *IEEE Trans. Signal Process.*, vol. 59, no. 7, pp. 3434–3440, Jul. 2011.

[26] L. Yang and K. C. Ho, "Alleviating sensor position error in source localization using calibration emitters at inaccurate locations," *IEEE Trans. Signal Process.*, vol. 58, no. 1, pp. 67–83, Jan. 2010.
[27] Z. Ma and K. C. Ho, "A study on the effects of sensor position error and the placement of calibration emitter for source localization," *IEEE Trans. Wireless Commun.*, vol. 13, no. 10, pp. 5440–5452, Oct. 2014.
[28] D. Wang, J. Yin, X. Chen, C. Jia, and F. Wei, "On the use of calibration emitters for TDOA source localization in the presence of synchronization clock bias and sensor location errors," *EURASIP J. Adv. Signal Process.*, vol. 2019, no. 1, pp. 1–34, 2019.
[29] D. Wang and Y. Wu, "Statistical performance analysis of direct position determination method based on Doppler shifts in presence of model errors," *Multidimensional Syst. Signal Process.*, vol. 28, no. 1, pp. 149–182, 2017.
[30] D. Wang, H. Yu, Z. Wu, and C. Wang, "Performance analysis of the direct position determination method in the presence of array model errors," *Sensors*, vol. 17, no. 7, 2017, Art. no. 1550.
[31] D. Wang, J. Yin, R. Liu, H. Yu, and Y. D. Wang, "Performance analysis and improvement of direct position determination based on Doppler frequency shifts in presence of model errors: Case of known waveforms," *Multidimensional Syst. Signal Process.*, vol. 30, no. 2, pp. 749–790, 2019.
[32] J. Yin, D. Wang, Y. Wu, and T. Tang, "Single-step localization using multiple moving arrays in the presence of observer location errors," *Signal Process.*, vol. 152, pp. 392–410, 2018.
[33] G. Wu, M. Zhang, and F. Guo, "Self-calibration direct position determination using a single moving array with sensor gain and phase errors," *Signal Process.*, vol. 173, 2020, Art. no. 107587.
[34] J. Yin, D. Wang, F. Nie, and N. Zheng, "Single-step geolocation for a non-circular source in the presence of satellite orbit perturbations," *IET Signal Process.*, vol. 16, no. 3, pp. 170–200, 2022.
[35] G. Wu, M. Zhang, and F. Guo, "On the use of a calibration emitter for direct position determination with single moving array in the presence of sensor gain and phase errors," *Digit. Signal Process.*, vol. 102, 2020, Art. no. 102734.
[36] Z. Yang, D. Wang, B. Yang, and F. Wei, "Robust direct position determination against sensor gain and phase errors with the use of calibration sources," *Multidimensional Syst. Signal Process.*, vol. 31, no. 3, pp. 1435–1468, 2020.
[37] A. J. Weiss, "Direct position determination of narrowband radio frequency transmitters," *IEEE Signal Process. Lett.*, vol. 11, no. 5, pp. 513–516, May 2004.
[38] P. Brémaud, *Markov Chains: Gibbs Fields, Monte Carlo Simulation, and Queues*, vol. 31. Berlin, Germany: Springer, 2013.
[39] Y. Xiong, N. Wu, Y. Shen, and M. Z. Win, "Cooperative network synchronization: Asymptotic analysis," *IEEE Trans. Signal Process.*, vol. 66, no. 3, pp. 757–772, Feb. 2018.
[40] Y. Xiong, N. Wu, Y. Shen, and M. Z. Win, "Cooperative localization in massive networks," *IEEE Trans. Inf. Theory*, vol. 68, no. 2, pp. 1237–1258, Feb. 2022.

Ming-Yi You received the B.S. and Ph.D. degrees in mechanical engineering from Shanghai Jiao Tong University, Shanghai, China, in 2006 and 2012, respectively.

From 2007 to 2008, he was invited to visit the M. S. Wu Manufacturing Research Center, University of Michigan, Ann Arbor, MI, USA. He is currently a Senior Expert with the No. 36 Research Institute of China Electronics Technology Group, Jiaxing, China, and leading a Research Group in radio direction finding and localization. He has authored or coauthored more than 50 articles and coauthored two books. His research interests include condition-based maintenance, radio direction finding, wireless localization, and multiobject tracking.

Wenqiang Pu (Member, IEEE) received the B.S. and Ph.D. degrees in electrical engineering from Xidian University, Xi'an, China, in 2013 and 2018, respectively.

From 2019 to 2020, he was a Postdoctoral Associate with the School of Science and Engineering, The Chinese University of Hong Kong, Shenzhen, China. He is currently a Research Scientist with the Shenzhen Research Institute of Big Data and an Adjunct Assistant Professor with the School of Science and Engineering, The Chinese University of Hong Kong, Shenzhen, China. His research interests include signal processing and optimization algorithms.

Dr. Pu was the recipient of the Best Student Paper Award from IEEE SAM 2024 for the paper he coauthored. He is currently an Associate Editor for IEEE SIGNAL PROCESSING LETTERS.

Rui Zhou (Member, IEEE) received the B.Eng. degree in information engineering from Southeast University, Nanjing, China, in 2017, and the Ph.D. degree in electronic and computer engineering from the Hong Kong University of Science and Technology, Hong Kong, in 2021.

He is currently a Research Scientist with the Shenzhen Research Institute of Big Data and an Adjunct Assistant Professor with the School of Science and Engineering, The Chinese University of Hong Kong, Shenzhen, China. His research interests include optimization algorithms, statistical signal processing, machine learning, and financial engineering.

Yun-Xia Ye received the B.S. and M.S. degrees in measurement technology and instruments from Xidian University, Xi'an, China, in 2012 and 2015, respectively.

She is currently a Senior Engineer with the No. 36 Research Institute of China Electronics Technology Group, Jiaxing, China. She has authored or coauthored more than ten articles and coauthored the book *Radio Direction Finding: Theory and Practice*. Her research interests include signal processing, radio direction finding, and wireless localization.

Minrui Xiao received the B.S. degree in measurement and control technology and instruments in 2022 from Shanghai Jiao Tong University, Shanghai, China, where she is currently working toward the M.S. degree in electrical and electronic engineering.

Her research focuses on emitter localization in complex scenarios.

Wei Wang received the Ph.D. degree in cryptography from Xidian University, Xi'an, China, in 2008.

He is currently the Executive Deputy Director with the Science and Technology on Communication Information Security Control Laboratory, Jiaxing, China. He has authored or coauthored 40 articles and three books. His research interests include wireless network control and communication information security control.

Qingjiang Shi (Member, IEEE) received the Ph.D. degree in electronic engineering from Shanghai Jiao Tong University, Shanghai, China, in 2011.

From 2009 to 2010, he visited Prof. Z.-Q. (Tom) Luo's research group with the University of Minnesota, Twin Cities, Minneapolis, MN, USA. In 2011, he was a Research Scientist with Bell Labs, Shanghai. In 2012, he was with the School of Information and Science Technology, Zhejiang Sci-Tech University. From 2016 to 2017, he was a Research Fellow with Iowa State University, Ames, IA, USA. Since 2018, he has been with the School of Software Engineering, Tongji University, Shanghai, where he is currently a Full Professor. He is also with the Shenzhen Research Institute of Big Data. So far, he has authored or coauthored more than 80 IEEE journals and filed about 40 national patents. His research interests include algorithm design and analysis with applications in machine learning, signal processing, and wireless networks.

Dr. Shi was an Associate Editor for IEEE TRANSACTIONS ON SIGNAL PROCESSING. He was the recipient of the IEEE Signal Processing Society Best Paper Award in 2022, the Huawei Technical Cooperation Achievement Transformation Award (2nd Prize) in 2022, the Huawei Outstanding Technical Achievement Award in 2021, the Golden Medal at the 46th International Exhibition of Inventions of Geneva in 2018, the First Prize of Science and Technology Award from China Institute of Communications in 2017, the National Excellent Doctoral Dissertation Nomination Award in 2013, the Shanghai Excellent Doctoral Dissertation Award in 2012, and the Best Paper Award from the IEEE PIMRC'09 conference.